

Designing a minimal Landau theory to stabilize desired quasicrystals

Wei Si,^{a, b ‡} Shifeng Li,^{a, c ‡} Pingwen Zhang,^{b, c *} An-Chang Shi,^{d *} and Kai Jiang^{a *}

^a *School of Mathematics and Computational Science,*

Hunan Key Laboratory for Computation and Simulation in Science

and Engineering, Xiangtan University, Hunan, 411105, China.

^b *LMAM, CAPT and School of Mathematical Sciences, Peking University, Beijing 100871, China.*

^c *School of Mathematics and Statistics, Wuhan University, Wuhan, 430072, China.*

^d *Department of Physics and Astronomy, McMaster University, Hamilton L8S 4M1, Canada.*

Interparticle interactions with multiple length scales play a pivotal role in the formation and stability of quasicrystals. Choosing a minimal set of length scales to stabilize a given quasicrystal is a challenging problem. To address this challenge, we propose an intelligent screening method (ISM) to design a Landau theory with a minimal number of length scales – referred to as the minimal Landau theory – that includes only the essential length scales necessary to stabilize quasicrystals. Based on a generalized multiple-length-scale Landau theory, ISM first evaluates various spectral configurations of candidate structures under a hard constraint. It then identifies the configuration with the lowest free energy. Using this optimal configuration, ISM calculates phase diagrams to explore the thermodynamic stability of desired quasicrystals. ISM can design a minimal Landau theory capable of stabilizing the desired quasicrystals by incrementally increasing the number of length scales. Our application of ISM has not only confirmed known behaviors in 10- and 12-fold quasicrystals but also led to a significant prediction that quasicrystals with 8-, 14-, 16-, and 18-fold symmetry could be stable within three-length-scale Landau models.

I. Introduction

Quasicrystals (QCs) are ordered structures that exhibit rotational symmetry but lack translational symmetry. Since the first discovery of QCs in Al-Mn alloys [1], QCs have attracted tremendous attention in material science and condensed matter physics [2–9]. In recent years, QCs have been discovered in a variety of soft condensed matter, including micelle-forming liquid crystals [3, 8, 10–12], block copolymers [4, 7, 13–16], colloidal suspensions [17], and binary mixtures of nanoparticles [18, 19]. To date, numerous QCs with 8-, 10-, 12-, and 18-fold rotational symmetries have been frequently

reported in both metallic alloys [2] and soft matters [3, 6–9, 13, 15, 17, 19–22]. Much effort has been devoted to studying the properties of QCs, predicting their stability, and developing methods to control their formation [23, 24].

Landau theories have been extensively employed to study the formation, stability and phase transition of ordered phases, including periodic crystals and QCs [25–29]. Generally, a Landau free-energy functional consists of a polynomial-type bulk energy and a nonlocal pairwise interaction,

$$\mathcal{F}[\phi(\mathbf{r})] = \int [d_2\phi(\mathbf{r})^2 + d_3\phi(\mathbf{r})^3 + d_4\phi(\mathbf{r})^4 + \dots] d\mathbf{r} + \frac{1}{2} \iint \phi(\mathbf{r}) C(|\mathbf{r} - \mathbf{r}'|) \phi(\mathbf{r}') d\mathbf{r} d\mathbf{r}', \quad (1)$$

where $\phi(\mathbf{r})$ is an order parameter describing the particle distribution, $C(r)$ is the correlation potential that

‡ These authors contributed equally to this work.

* Corresponding authors. E-mail addresses: pzhang@pku.edu.cn

(P. Zhang), shi@mcmaster.ca (A.-C. Shi), kaijiang@xtu.edu.cn

(K. Jiang).

is finite for the distance r between particles [30]. $f = \lim_{\Omega \rightarrow \mathbb{R}^3} \frac{1}{V(\Omega)} \int_{\Omega} \dots$ and $V(\Omega)$ is the volume of the region Ω . In the case of a periodic phase, the integral is equivalent to an integral over its unit cell. The power series in the first term of Eq. (1) is typically truncated to the fourth order [31–33]. The quadratic term contributes to the growth of instability, while the quartic term establishes a lower bound for the free energy. The cubic term breaks the $\phi \rightarrow -\phi$ symmetry.

An understanding of how to stabilize an ordered structure comes from representing the second term of (1) in reciprocal space,

$$\frac{1}{2} \int \hat{C}(k) |\hat{\phi}(\mathbf{k})|^2 d\mathbf{k}, \quad k = |\mathbf{k}|,$$

where \mathbf{k} is the reciprocal lattice vector (RLV), $\hat{\phi}(\mathbf{k}) = \int \exp(-i\mathbf{k} \cdot \mathbf{r}) \phi(\mathbf{r}) d\mathbf{r}$ is the Fourier transform of $\phi(\mathbf{r})$, and $\hat{C}(k)$ is the Fourier transform of $C(r)$. The Fourier coefficients $\hat{\phi}(\mathbf{k})$ with wave numbers at the minima of $\hat{C}(k)$ are energetically favored. Given the N -fold rotational symmetry, the correlation potential can be approximated by a polynomial with roots d_1, d_2, \dots ,

$$\hat{C}(k) \approx c(k^2 - d_1^2)(k^2 - d_2^2) \dots, \quad c > 0. \quad (2)$$

When $\hat{C}(k)$ is truncated to second order, i.e., $c(k^2 - d_1^2)$, which has the minima at $k = 0$, the model can be used to simulate the solidification process of binary mixtures, such as phase-field models [34].

More complex phase behaviors related to multiple length scales can be investigated by the correlation potential with multiple roots [31–33, 35–37]. For a single length scale, the potential (2) should be truncated to fourth order and rewritten as $c(k^2 - 1)^2$ by scaling k in units of $\sqrt{(d_1^2 + d_2^2)/2}$ and omitting constant terms. This potential discourages RLVs with wave numbers deviating from the length scale 1. The single-length-scale potential has been extensively utilized to explain phase behaviors in periodic systems, such as Landau-Brazovskii model [31] and Swift-Hohenberg model [32]. To achieve two length scales, $\hat{C}(k)$ must be truncated to eighth order and rewritten as $c[(k^2 - q_1^2)(k^2 - q_2^2)]^2$, which features

two equal-depth minima at $k = q_1$ and $k = q_2$. This two-length-scale potential was firstly proposed by Lifshitz and Petrich (LP) to describe quasiperiodic pattern-forming dynamics [33] and to find stable 12-fold QCs by setting $q_2/q_1 = 2 \cos(\pi/12)$. Over the years, this two-length-scale type potential has been widely used to study the thermodynamic stability of QCs and found stable 10-, 12-fold QCs and three-dimensional icosahedral QCs [5, 35–43].

However, many QCs are metastable or unstable in two-length-scale models, such as 8- and 18-fold QCs. This raises the question: could these QCs be stabilized by introducing more length scales? Lifshitz and Petrich speculated that correlation potentials with three or four length scales could stabilize higher-order symmetric QCs, such as 18- or 24-fold QCs [33]. Savitz *et al.* have demonstrated that this conjecture might be correct and found stable 8- and 18-fold QCs in four-length-scale Landau models [36]. However, increasing the number of length scales introduces greater complexity in interparticle interactions within physical systems and poses a significant challenge for theoretical analysis [3, 13, 15, 44, 45]. Therefore, it is crucial to design a Landau theory with the minimal number of length scales, i.e., the minimal Landau model to stabilize desired QCs.

Designing a minimal Landau theory requires a general Landau model with multiple length scales. To incorporate m length scales, we could truncate Eq. (2) to the $4m$ -th order and adjust parameters to achieve equal-depth minima at $k = q_1, \dots, q_m$, thereby rewriting the correlation potential in the form,

$$\hat{C}_m(k) = c \left[\prod_{j=1}^m (k^2 - q_j^2) \right]^2, \quad c > 0. \quad (3)$$

This pair potential favors the RLVs with wave numbers close to the length scales q_1, \dots, q_m but suppresses the other RLVs. Substituting Eq. (3) into Eq. (1) and truncating the polynomial to fourth order lead to a general-

ized m -length-scale free-energy functional [36, 45]

$$\begin{aligned} \mathcal{F}_m[\phi(\mathbf{r})] = & \int \left(-\frac{\epsilon}{2}\phi^2 - \frac{\alpha}{3}\phi^3 + \frac{1}{4}\phi^4 \right) d\mathbf{r} \\ & + \frac{c}{2} \int \left[\prod_{j=1}^m (\nabla^2 + q_j^2)\phi(\mathbf{r}) \right]^2 d\mathbf{r}, \end{aligned} \quad (4)$$

where the parameter ϵ is temperature-related, α measures the intensity of three-body interaction, $c > 0$ is a penalty factor, and q_1, \dots, q_m are length scales. The function $\phi(\mathbf{r})$ satisfies the mean-zero constraint, $\int \phi(\mathbf{r}) d\mathbf{r} = 0$, corresponding to a mass-conserved system.

We organize the rest of this paper as follows. In Section II, we propose an intelligent screening method to design a minimal Landau theory for desired QCs. In Section III, we apply this method to design minimal Landau theories for $2n$ -fold QCs ($n = 4, 5, \dots, 9$). We find that three-length-scale Landau models can stabilize 8-, 14-, 16-, and 18-fold QCs. Finally, we summarize this work in Section IV.

II. Intelligent screening method (ISM)

Designing a minimal Landau theory to stabilize desired QCs requires considering various candidate structures. For a candidate phase, there are numerous possible configurations of RLVs describing its spectral distribution. To identify the optimal configuration with the lowest free energy, it is crucial to analyze the contributions of RLVs.

RLVs could be categorized into primary and non-primary RLVs. The primary RLVs exhibit strong intensities and have wave numbers equal to length scales. The remaining RLVs are the non-primary RLVs. Numerous studies indicate that the primary RLVs determine the main characteristics of ordered structures and the non-primary RLVs influence local details [35, 36, 41, 46]. The contributions of primary and non-primary RLVs can be studied from two perspectives: hard constraint (HC) with $c \rightarrow \infty$, and soft constraint (SC) with a finite c . Under the HC, $\hat{C}_m(k)$ is zero if the wave number k belongs to the set $\{q_1, \dots, q_m\}$, and otherwise it is infinite. This implies that all non-primary RLVs are forbidden

under this constraint. The SC relaxes the restriction on wave numbers, permitting the emergence of non-primary RLVs, which may be favored by a realistic system.

Based on the two constraints, we propose ISM to design a minimal Landau theory to stabilize the desired QCs, as shown in Fig. 1. Given a target QC and the number of length scales, there might be many configurations of primary RLVs. Let us consider HC first. For a specific configuration, HC only allows a finite number of primary RLVs, thus the free energy functional can be written as a polynomial function. The polynomial function can be easily minimized by computer-assisted symbolic calculation to obtain the free energy of the configuration. Among all configurations, ISM selects the optimal one with the lowest free energy by directly comparing the free energies. Using the optimal configuration, we can study the thermodynamic stability of the target QC by constructing phase diagrams under HC. If the target QC is metastable or unstable, we increase the number of length scales to obtain more configurations. The optimal configuration among these may lead to the formation of stable QC. The free energy functional \mathcal{F}_m with these length scales is called a HC minimal Landau model. Based on the optimal configuration and the HC minimal Landau model, we further design a minimal Landau model under SC. Since SC permits the emergence of non-primary RLVs, we use numerical methods to calculate SC phase diagrams to study the stability of target QC. We obtain the SC minimal Landau model if the target QC is stable, otherwise, we repeat the above process with more length scales. We can always obtain a minimal Landau theory to stabilize target QC since more length scales have more primary RLVs that may form more triplets to lower the free energy.

In order to obtain the possible configurations of primary RLVs, we first analyze the elements of primary RLVs. For a candidate phase, its primary RLVs are determined by the length scales and the relative positions. As an example, we consider two-length-scale 8-fold QCs,

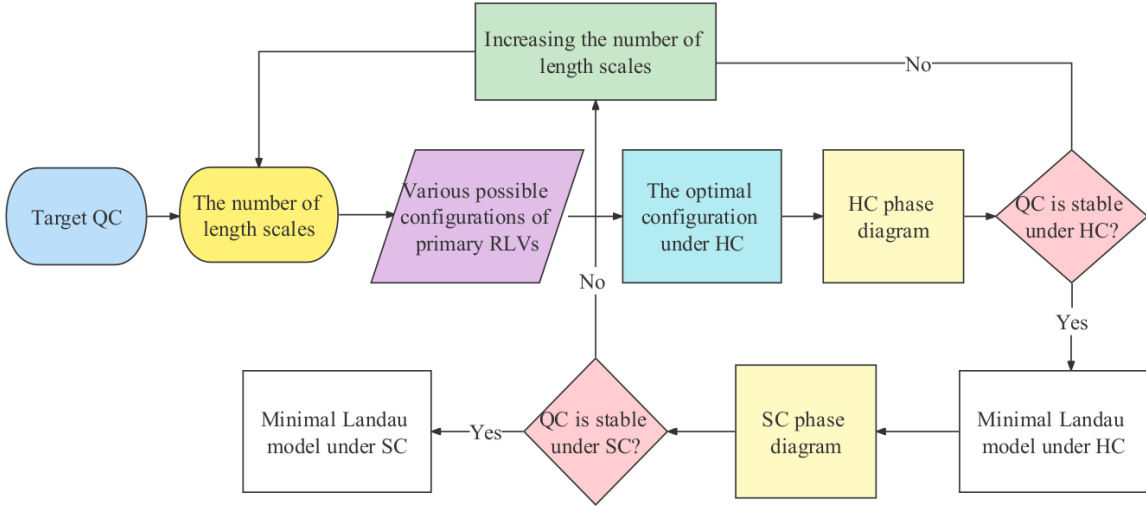


FIG. 1. Flowchart of ISM. The number of length scales increases gradually from 1.

as demonstrated in Fig. 2. The length scales are consistent with the radii of the circles q_1 and q_2 . The relative positions depend on the offset angles θ_1 and θ_2 . The offset angle of each circle is defined as the minimal angle at which the primary RLV rotates clockwise in the horizontal direction. Note that the primary RLVs on each circle are equivalent due to rotational symmetry. Without loss of generality, we set $\theta_1 = 0$ and the rest is $\theta_2 - \theta_1$. For an m -length-scale N -fold candidate phase, we have

$$q_j = \cos(w_j \pi / N), \quad j = 1, \dots, m, \quad (5)$$

$$\theta_1 = 0, \quad \theta_{j'} = s_{j'} \pi / N, \quad j' = 2, \dots, m. \quad (6)$$

The primary RLVs given by (5) and (6) can form more triplets, which could lower the free energy. $w_j \in [0, N/2)$ due to the periodicity of the cosine function, and $s_{j'} \in [0, 2)$ because of rotational symmetry. We obtain various possible configurations of primary RLVs by discretizing w_j and $s_{j'}$ in the valid ranges.

Under HC, the free energy functional \mathcal{F}_m can be written as a polynomial function. Since $\hat{C}_m(k)$ should be zero to ensure finite free energy, \mathcal{F}_m preserves bulk energy part

$$\mathcal{F}_m = \int \left(-\frac{\epsilon^*}{2} \phi^2 - \frac{1}{3} \phi^3 + \frac{1}{4} \phi^4 \right) d\mathbf{r}, \quad (7)$$

where $\epsilon^* = \epsilon/\alpha^2$. Note that Eq. (7) has scaled the cubic coefficient α to unity by measuring the field ϕ in units

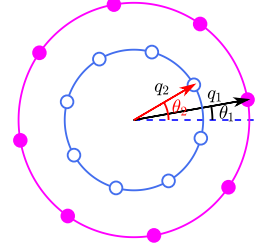


FIG. 2. Primary RLVs of the 8-fold QC with two length scales q_1 and q_2 . Magenta (royal blue) dots and the origin form the primary RLVs. θ_1 and θ_2 are offset angles.

of α and the energy in units of α^4 . Using the Fourier transformation of $\phi(\mathbf{r})$, Eq. (7) becomes

$$\begin{aligned} \mathcal{F}_m(\hat{\phi}_{q_1}, \dots, \hat{\phi}_{q_m}) &= -\frac{\epsilon^*}{2} \sum_{\mathbf{k}_1 + \mathbf{k}_2 = \mathbf{0}} \hat{\phi}_{\mathbf{k}_1} \hat{\phi}_{\mathbf{k}_2} \\ &\quad - \frac{1}{3} \sum_{\mathbf{k}_1 + \mathbf{k}_2 + \mathbf{k}_3 = \mathbf{0}} \hat{\phi}_{\mathbf{k}_1} \hat{\phi}_{\mathbf{k}_2} \hat{\phi}_{\mathbf{k}_3} \\ &\quad + \frac{1}{4} \sum_{\mathbf{k}_1 + \mathbf{k}_2 + \mathbf{k}_3 + \mathbf{k}_4 = \mathbf{0}} \hat{\phi}_{\mathbf{k}_1} \hat{\phi}_{\mathbf{k}_2} \hat{\phi}_{\mathbf{k}_3} \hat{\phi}_{\mathbf{k}_4}, \end{aligned} \quad (8)$$

where all $k_i = |\mathbf{k}_i|$ belong to the set $\{q_1, \dots, q_m\}$, $i = 1, 2, 3, 4$, and $\hat{\phi}_{q_j}$ denotes the Fourier coefficient with wave number q_j . In Eq. (8), the three-RLV interaction in the third row is beneficial to lower the free energy, but the four-RLV interaction in the fourth row increases the free energy. Since the primary RLVs are finite for a specific

configuration, we can calculate the summations in Eq. (8) by symbolic computation. We then minimize the polynomial function with respect to $\hat{\phi}_{q_1}, \dots, \hat{\phi}_{q_m}$ to obtain the free energy of this configuration. Among all possible configurations, we select the optimal configuration with the lowest free energy. Using the optimal configuration, we study the thermodynamic stability of desired QCs by constructing a phase diagram under HC.

Under SC, ISM can also examine the thermodynamic stability of desired QCs by combining with numerical methods. An accurate and efficient numerical approach to study QCs is the projection method [47, 48]. The projection method embeds the QC into a high-dimensional periodic system which can be efficiently calculated by fast Fourier transformation, and then obtains the QC by projecting it back to the original space. The specific formula of the projection method is

$$\phi(\mathbf{r}) = \sum_{\mathbf{h} \in \mathbb{Z}^{d_1}} \hat{\phi}(\mathbf{h}) e^{i(\mathcal{P} \cdot \mathbf{h})^T \cdot \mathbf{r}}, \quad \mathbf{r} \in \mathbb{R}^{d_0}, \quad d_0 \leq d_1, \quad (9)$$

where \mathcal{P} is a $d_0 \times d_1$ -order projection matrix. d_0 is the dimension of the original space, and d_1 is the dimension of the high-dimensional space dependent on the symmetry of the QC. A special case of $d_0 = d_1$ implies that the projection method is the common Fourier pseudo-spectral approach for periodic crystals. Moreover, the m -length-scale model under SC can be rescaled to reduce the number of model parameters. Let q_* be any element of the set $\{q_j\}_{j=1}^m$. c is rescaled to unit by measuring the field ϕ in units of $\sqrt{c}q_*^{2m}$, and consequently the energy is measured in units of $c^2q_*^{8m}$, thus Eq. (4) becomes

$$\mathcal{F}_m[\phi(\mathbf{r})] = \int \left(-\frac{\epsilon}{2}\phi^2 - \frac{\alpha}{3}\phi^3 + \frac{1}{4}\phi^4 \right) d\mathbf{r} + \frac{1}{2} \int \left[\prod_{j=1}^m (\nabla^2 + q_j^2/q_*^2)\phi(\mathbf{r}) \right]^2 d\mathbf{r}, \quad (10)$$

where ϵ and α are measured in units of cq_*^{4m} and $\sqrt{c}q_*^{2m}$, respectively. In this work, q_* takes the minimal value of $\{q_j\}_{j=1}^m$. Its stationary solutions can be quickly and robustly obtained by recently developed optimization methods [49–51]. And its phase diagram can be automat-

ically and efficiently generated by our developed open-source software [52].

III. Results and discussions

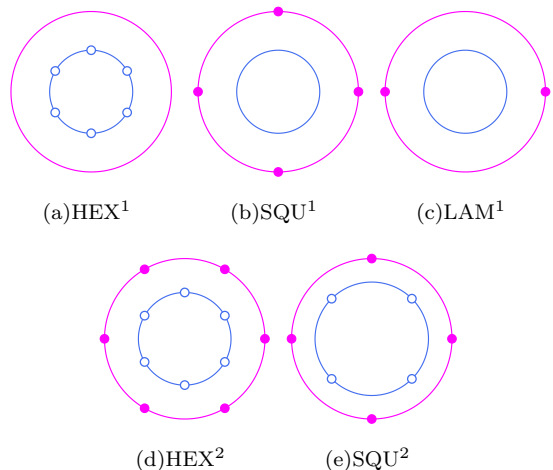


FIG. 3. Optimal primary RLVs of (a)-(c) single-length-scale and (d)-(e) two-length-scale competing crystals. Superscripts denote the number of valid length scales. The radius of inner (royal blue) circle is q_1 and the radius of outer (magenta) circle is q_2 . q_2/q_1 is equal to (d) $2 \cos(\pi/6)$; (e) $2 \cos(\pi/4)$.

Applying the ISM, we design minimal Landau theories for two-dimensional $2n$ -fold QCs ($n = 4, 5, \dots, 9$). These QCs are named as octagonal (O), decagonal (D), dodecagonal (DD), tetradecagonal (TD), hexadecagonal (HD) and octadecagonal (OD) QCs, respectively. Note that the primary RLVs with a single length scale could not generate sufficient three-RLV interactions to stabilize QCs in the Landau free-energy functionals [33, 46]. We present the numerical results of two, three and four length scales in Supplementary Material (SM). The results include optimal configurations of primary RLVs, HC free energy, HC phase diagrams, and the SC phase diagrams of minimal Landau models. The results demonstrate that 10- and 12-fold QCs can be stabilized in the Landau model with at least two length scales, which is consistent with previous findings [33, 35, 39–41], implying the effectiveness of ISM. The results of 8-, 14-, 16- and 18-fold QCs give some exciting predictions, which will be introduced in this section.

In what follows, we consider three competing crystals, including lamellar (LAM), square (SQU) and hexagonal (HEX) crystals to study the thermodynamic stability of an m -length-scale QC. The competing crystals have the length scales consistent with the length scales of the QC. The offset angles follow Eq. (6), where $N = 2$ for LAM, $N = 4$ for SQU, and $N = 6$ for HEX. Under HC, the free energy functional can be written as a polynomial function, thus we can easily obtain the optimal primary RLVs of these crystals. It should be noted that if the Fourier coefficients at some primary RLVs are very weak or even vanished, i.e., these primary RLVs become non-primary RLVs, the number of valid length scales of the crystals denoted by superscripts is less than m . Numerical simulations demonstrate the optimal configuration of primary RLVs has one or two valid length scales for HEX and SQU but only one valid length scale for LAM, as shown in Fig. 3. For the case of one valid length scale, the HC free energies are

$$\mathcal{F}_{\text{HEX}^1}(\hat{\phi}_j, \epsilon^*) = -3\epsilon^* \hat{\phi}_j^2 - 4\hat{\phi}_j^3 + \frac{45}{2}\hat{\phi}_j^4, \quad (11)$$

$$\mathcal{F}_{\text{SQU}^1}(\hat{\phi}_j, \epsilon^*) = -2\epsilon^* \hat{\phi}_j^2 + 9\hat{\phi}_j^4, \quad (12)$$

$$\mathcal{F}_{\text{LAM}^1}(\hat{\phi}_j, \epsilon^*) = -\epsilon^* \hat{\phi}_j^2 + \frac{3}{2}\hat{\phi}_j^4. \quad (13)$$

For the case of two valid length scales, the length scales satisfy a special ratio to form more three-RLV interactions: $q_2/q_1 = 2 \cos(\pi/6)$ for HEX² and $q_2/q_1 = 2 \cos(\pi/4)$ for SQU². Their HC free energies are given by

$$\begin{aligned} \mathcal{F}_{\text{HEX}^2}(\{\hat{\phi}_j\}_{j=1}^2, \epsilon^*) &= -3\epsilon^*(\hat{\phi}_1^2 + \hat{\phi}_2^2) - 12\hat{\phi}_1^2\hat{\phi}_2 \\ &- 4\hat{\phi}_1^3 - 4\hat{\phi}_2^3 + \frac{45}{2}(\hat{\phi}_1^4 + \hat{\phi}_2^4) + 36\hat{\phi}_1^3\hat{\phi}_2 + 90\hat{\phi}_1^2\hat{\phi}_2^2, \end{aligned} \quad (14)$$

$$\begin{aligned} \mathcal{F}_{\text{SQU}^2}(\{\hat{\phi}_j\}_{j=1}^2, \epsilon^*) &= -2\epsilon^*(\hat{\phi}_1^2 + \hat{\phi}_2^2) - 8\hat{\phi}_1^2\hat{\phi}_2 \\ &+ 9(\hat{\phi}_1^4 + 4\hat{\phi}_1^2\hat{\phi}_2^2 + \hat{\phi}_2^4). \end{aligned} \quad (15)$$

A. Octagonal (O) QCs

Two-dimensional OQCs have been frequently observed in materials since the first discovery in V-Ni-Si and Cr-

Ni-Si alloys [53]. Their electron-diffraction patterns reveal that OQCs have multiple length scales [53]. Theoretical studies have pointed out that the formation of OQCs may require correlation potentials with multiple length scales. Concretely, the two-length-scale Landau model, such as the LP model, could obtain a metastable OQC [41], and the four-length-scale model could stabilize OQC [36]. In this section, we apply the ISM and design a minimal Landau theory to stabilize OQC.

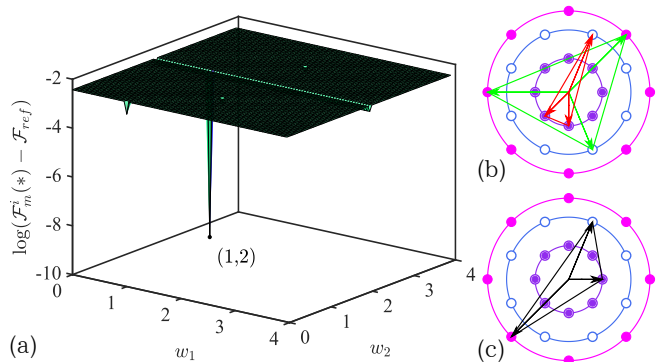


FIG. 4. (a) Free energies of OQC³ as a function of w_1 and w_2 . $w_3 = 3$, $s_2 = 1$, $s_3 = 0$. $\mathcal{F}_m^i(*)$ is the minimal value of the HC model with $\epsilon^* = 0$. $(w_1, w_2) = (1, 2)$ is the peak point with free energy $\mathcal{F}_{ref} = -3.7285 \times 10^{-3}$. At the peak point, the primary RLVs with length scales $\cos(\pi/8)$, $\cos(\pi/4)$, $\cos(3\pi/8)$ have two types of three-RLV interactions, as shown in (b)-(c).

ISM firstly finds the optimal configuration of primary RLVs of m -length-scale OQC. The length scales and offset angles are

$$q_j = \cos(w_j \pi/8), \quad w_j \in [0, 4), \quad j = 1, \dots, m,$$

$$\theta_1 = 0, \quad \theta_{j'} = s_{j'} \pi/8, \quad s_{j'} \in [0, 2), \quad j' = 2, \dots, m.$$

For a specific configuration involving variables $w_1^i, \dots, w_m^i, s_2^i, \dots, s_m^i$, the Landau model is written as a polynomial with the minimal value $\mathcal{F}_m^i(*)$. The configuration yielding the lowest $\mathcal{F}_m^i(*)$ is considered optimal. Taking $m = 3$ as an example, Fig. 4(a) plots $\mathcal{F}_m^i(*)$ against w_1 and w_2 when fixing $w_3 = 3$, $s_2 = 1$, and $s_3 = 0$. The energy surface is almost flat except for a few peaks. This implies that only a few

configurations can significantly lower free energies. The lowest peak whose energy is denoted as \mathcal{F}_{ref} occurs at $(w_1, w_2) = (1, 2)$. The corresponding primary RLVs have length scales of $\cos(\pi/8)$, $\cos(\pi/4)$, and $\cos(3\pi/8)$. We have confirmed that this configuration remains optimal as w_3 , s_2 and s_3 change. In this optimal configuration, there are two different ways to form the three-RLV interaction. One involves two RLVs with equal wave numbers and another RLV with a different wave number, as illustrated in Fig. 4 (b). Another way involves three RLVs with different wave numbers, as shown in Fig. 4 (c). The HC free energy of the optimal configuration has the following expression

$$\begin{aligned} \mathcal{F}_{\text{OQC}^3}(\{\hat{\phi}\}_{j=1}^3, \epsilon^*) &= -4\epsilon^* \sum_{j=1}^3 \hat{\phi}_j^2 - 16\hat{\phi}_2(\hat{\phi}_1 + \hat{\phi}_3)^2 \\ &+ 42 \sum_{j=1}^3 \hat{\phi}_j^4 + 192\hat{\phi}_1\hat{\phi}_2\hat{\phi}_3 + 48\hat{\phi}_1\hat{\phi}_3(\hat{\phi}_1^2 + \hat{\phi}_3^2) \\ &+ 144(\hat{\phi}_1^2\hat{\phi}_2^2 + \hat{\phi}_1^2\hat{\phi}_3^2 + \hat{\phi}_2^2\hat{\phi}_3^2). \end{aligned} \quad (16)$$

Moreover, for $m = 2$, the optimal primary RLVs of OQC have length scales of 1 and $\cos(\pi/4)$, which are depicted in the embedded pattern of Fig. 5 (a), with the HC free energy expressed as

$$\begin{aligned} \mathcal{F}_{\text{OQC}^2}(\{\hat{\phi}\}_{j=1}^2, \epsilon^*) &= -4\epsilon^* \sum_{j=1}^2 \hat{\phi}_j^2 - 16\hat{\phi}_1\hat{\phi}_2^2 \\ &+ 42 \sum_{j=1}^2 \hat{\phi}_j^4 + 120\hat{\phi}_1^2\hat{\phi}_2^2. \end{aligned} \quad (17)$$

To study the thermodynamic stability of OQCs under HC, Fig. 5 (a) plots the HC free energy of candidate structures as a function of ϵ^* for a Landau model with two length scales 1 and $\cos(\pi/4)$. We find that SQU^2 is favorable when $\epsilon^* \leq 0.7688$, HEX^1 for $0.7688 \leq \epsilon^* \leq 1.9159$, and LAM^1 when $\epsilon^* \gtrsim 1.9159$. Thus the two-length-scale OQC is metastable. For a Landau model with three length scales $\cos(\pi/8)$, $\cos(\pi/4)$, and $\cos(3\pi/8)$, we find stable OQCs when $\epsilon^* \leq 0.0300$, as shown in Fig. 5 (b). The reason could be attributed that the primary RLVs in the three-length-scale OQC form more three-RLV interactions than those in the two-length-scale OQC, thereby

reducing the HC free energy. Furthermore, the HC phase diagram in the ϵ - α plane is plotted in Fig. 5 (c). Here, the three-length-scale OQC is expected to be thermodynamic stable when $-0.1021 \leq \epsilon^* \leq 0.0300$. Therefore, this three-length-scale Landau model is the minimal model to stabilize OQC under HC.

Based on the HC minimal Landau model, we further study the thermodynamic stability of OQC under SC to design a SC minimal Landau theory. We apply the projection method to evaluate OQCs and their free energies accurately. Fig. 6 (a₁) depicts the coordinates of the optimal primary RLVs of OQCs in two-dimensional space. To be consistent with the rescaling model (10), the length scales are measured in units of q_3 . We set the four vectors $(1, 0)$, $(\sqrt{2}/2, \sqrt{2}/2)$, $(0, 1)$, $(-\sqrt{2}/2, \sqrt{2}/2)$ as basis vectors, allowing the primary RLVs to be expressed by integer coefficients with the four vectors, as illustrated in Fig. 6 (a₂). Accordingly, the projection matrix is

$$\mathcal{P}_{\text{OQC}} = \begin{pmatrix} 1 & \sqrt{2}/2 & 0 & -\sqrt{2}/2 \\ 0 & \sqrt{2}/2 & 1 & \sqrt{2}/2 \end{pmatrix}. \quad (18)$$

The OQC is embedded into a four-dimensional periodic structure that can be accurately calculated, and then it is recovered by projecting this four-dimensional periodic structure into the two-dimensional space.

In Fig. 6 (a)-(d), we present the diffraction patterns and real-space morphologies of stationary candidate structures. Fig. 6 (e) presents the SC phase diagram, where OQC^3 , HEX^1 , and LAM^1 occupy stable regions but SQU^1 remains metastable. The phase boundaries in the SC phase diagram are similar to those in the HC phase diagram Fig. 5 (c). It may be attributed to the fact that the primary RLVs play a dominant role in determining the stability of candidate structures and the contribution of non-primary RLVs causes slight changes in phase boundaries. Consequently, we could come to a conclusion that the minimal Landau theory to stabilize OQCs under SC involves three length scales $\cos(\pi/8)$, $\cos(\pi/4)$, and $\cos(3\pi/8)$.

In previous work on primary RLVs of OQCs, only a

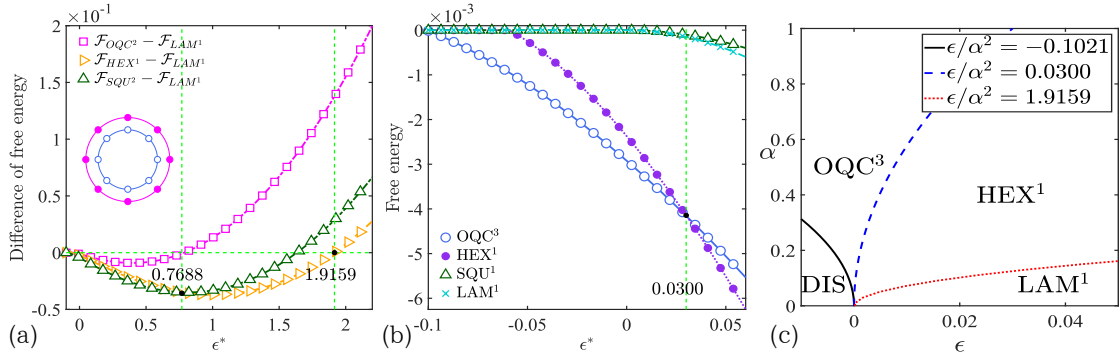


FIG. 5. (a) HC free energy of two-length-scale candidate phases with the energy of LAM^1 as the baseline. Two length scales are 1 and $\cos(\pi/4)$. The embedded pattern is the optimal primary RLVs of OQC^2 . (b) Free energies of candidate structures in the HC model with three length scales $\cos(\pi/8)$, $\cos(\pi/4)$, and $\cos(3\pi/8)$. (c) HC phase diagram of the three-length-scale model in ϵ - α plane. DIS stands for the disordered phase with zero free energy.

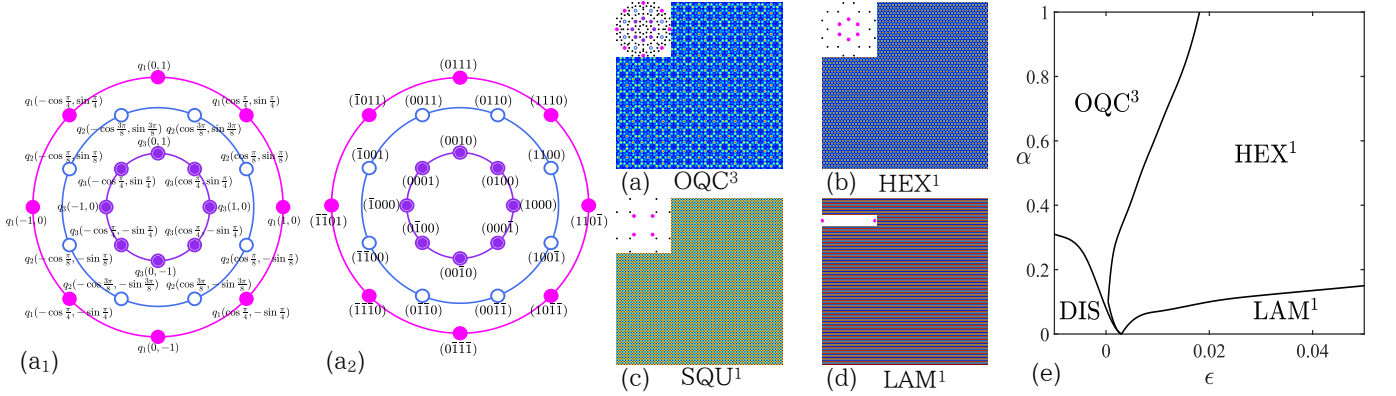


FIG. 6. Coordinates of optimal primary RLVs of OQC^3 in (a₁) two-dimensional and (a₂) four-dimensional reciprocal space. Stationary ordered states: (a) OQC^3 ; (b) HEX^1 ; (c) SQU^1 ; (d) LAM^1 calculated by the projection method in the Landau model with three length scales $\cos(\pi/8)$, $\cos(\pi/4)$ and $\cos(3\pi/8)$. The diffraction pattern embedded in the upper left corner only plots these RLVs with intensities greater than 10^{-6} . (e) SC phase diagram of the three-length-scale model.

finite number of configurations were considered [36, 54]. ISM examines nearly all possible configurations and effectively identifies the optimal configuration. Therefore, ISM can design a minimal Landau theory to stabilize OQCs.

B. Tetradecagonal (TD), Hexadecagonal (HD) and Octadecagonal (OD) QCs

To the best of our knowledge, TDQC and HDQC have not yet been observed in nature and laboratories. Utilizing ISM, we design minimal Landau theories to stabilize these structures, which may be helpful for experimental research. Numerical results demonstrate that the mini-

mal Landau theories both have three length scales.

For the three-length-scale TDQC, we present its optimal configuration of primary RLVs in Fig. 7(a). The corresponding HC free energy is

$$\begin{aligned}
 \mathcal{F}_{TDQC^3}(\{\hat{\phi}\}_{j=1}^4, \epsilon^*) &= -7\epsilon^* \sum_{j=1}^3 \hat{\phi}_j^2 - 56\hat{\phi}_1\hat{\phi}_2\hat{\phi}_3 \\
 &- 28(\hat{\phi}_1^2\hat{\phi}_3 + \hat{\phi}_1\hat{\phi}_2^2 + \hat{\phi}_2\hat{\phi}_3^2) + \frac{273}{2} \sum_{j=1}^3 \hat{\phi}_j^4 \\
 &+ 252\hat{\phi}_1\hat{\phi}_2\hat{\phi}_3 \sum_{j=1}^3 \hat{\phi}_j + 84(\hat{\phi}_1^3\hat{\phi}_2 + \hat{\phi}_1\hat{\phi}_3^3 + \hat{\phi}_2^3\hat{\phi}_3) \\
 &+ 378(\hat{\phi}_1^2\hat{\phi}_2^2 + \hat{\phi}_1^2\hat{\phi}_3^2 + \hat{\phi}_2^2\hat{\phi}_3^2).
 \end{aligned} \tag{19}$$

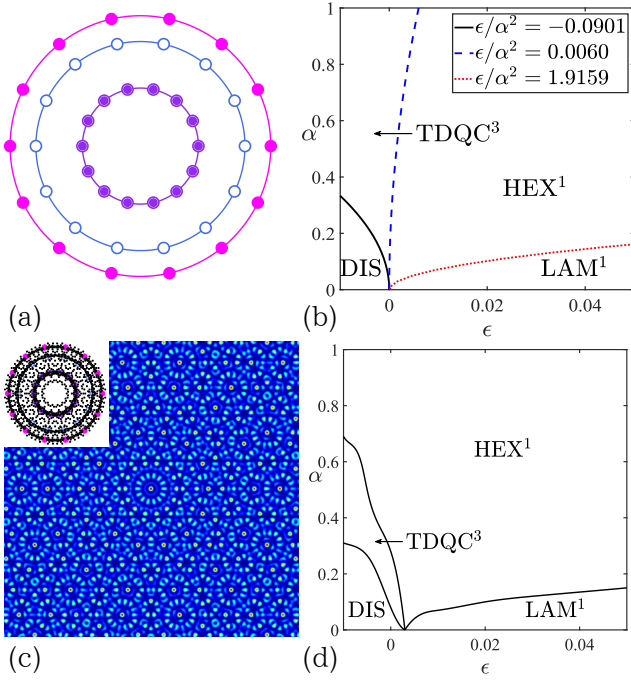


FIG. 7. (a) Optimal primary RLVs of TDQC³, (b) HC phase diagram, (c) stationary patterns of TDQC³ at $\epsilon = -0.01$ and $\alpha = 0.5$, (d) SC phase diagram. The three length scales are $\cos(\pi/14)$, $\cos(3\pi/14)$, and $\cos(5\pi/14)$.

Fig. 7(b) plots the HC phase diagram, where TDQC³ is stable when $-0.0901 \leq \epsilon^* \leq 0.0060$. Under SC, Fig. 7(c) displays the stationary patterns of TDQC³ computed by the projection method. More details on the projection matrix and high-dimensional coordinates can be found in SM Eq. (25) and Fig. 10(d), respectively. Fig. 7(d) shows the SC phase diagram, revealing a stable region for TDQC³.

For the three-length-scale HDQC, Fig. 8(a) presents the optimal configuration of primary RLVs, which results in the HC free energy

$$\begin{aligned} \mathcal{F}_{\text{HDQC}^3}(\{\hat{\phi}_j\}_{j=1}^4, \epsilon^*) &= -8\epsilon^* \sum_{j=1}^3 \hat{\phi}_j^2 - 32\hat{\phi}_2(\hat{\phi}_1 + \hat{\phi}_3)^2 \\ &+ 180 \sum_{j=1}^3 \hat{\phi}_j^4 + 96\hat{\phi}_1\hat{\phi}_3(\hat{\phi}_1^2 + \hat{\phi}_3^2) + 384\hat{\phi}_1\hat{\phi}_2^2\hat{\phi}_3 \\ &+ 480(\hat{\phi}_1^2\hat{\phi}_2^2 + \hat{\phi}_1^2\hat{\phi}_3^2 + \hat{\phi}_2^2\hat{\phi}_3^2). \end{aligned} \quad (20)$$

We plot the corresponding HC phase diagram in

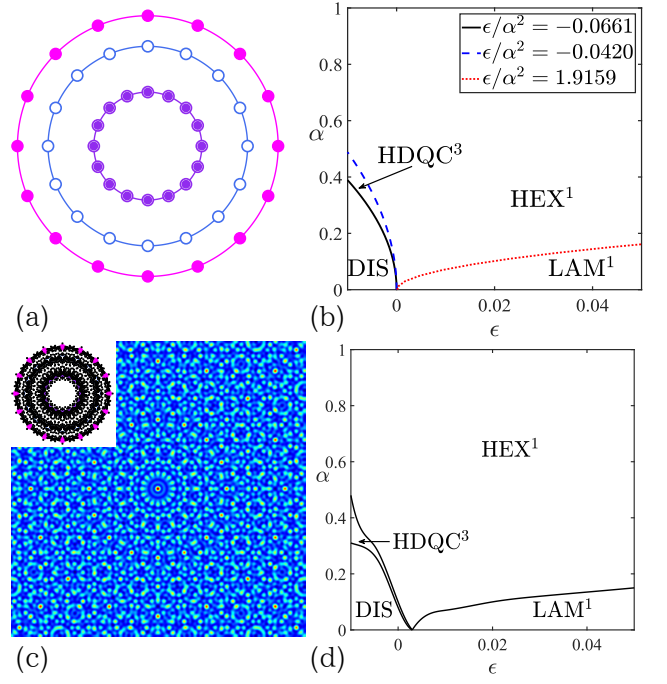


FIG. 8. (a) Optimal primary RLVs of HDQC³, (b) HC phase diagram, (c) stationary patterns at $\epsilon = -0.01$ and $\alpha = 0.4$, (d) SC phase diagram. The three length scales are $\cos(\pi/4)$, $\cos(\pi/8)$, and $\cos(3\pi/8)$.

Fig. 8(b), indicating that HDQC³ is thermodynamic stable for $-0.0661 \leq \epsilon^* \leq -0.0420$. Under SC, we use the projection method and obtain the stationary pattern of HDQC³ as shown in Fig. 8(c). We give the projection matrix in SM Eq. (26) and high-dimensional coordinates of HDQC³ in SM Fig. 10(e). Fig. 8(d) plots the SC phase diagram, confirming the stability of HDQC³ under SC.

ODQC has been discovered in soft colloidal systems, as evidenced by their diffraction patterns that exhibit multiple length scales [17]. Stable ODQCs in theoretical study have been obtained by a Landau model with four length scales [36]. In our study, we design three minimal Landau models by ISM, each with three different length scales: (I) $\cos(\pi/18)$, $\cos(2\pi/9)$, $1/2$; (II) $\cos(\pi/9)$, $\cos(5\pi/18)$, $1/2$; (III) $1/2$, $\cos(7\pi/18)$, $\cos(4\pi/9)$. Fig. 9(I)-(III) show the optimal configurations of primary RLVs of ODQCs, corresponding to the minimal models (I)-(III) respectively. These configurations have the same num-

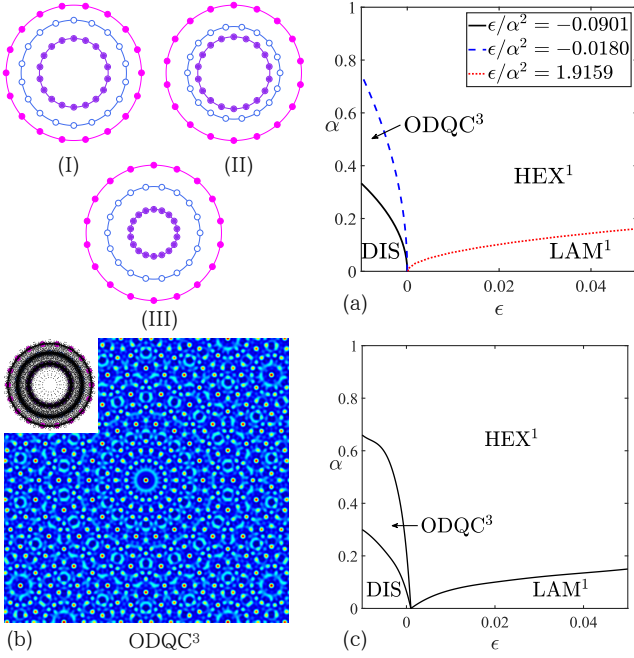


FIG. 9. Optimal primary RLVs of ODQC³ whose radii of the circles from outside to inside are (I) $\cos(\pi/18)$, $\cos(2\pi/9)$, $1/2$; (II) $\cos(\pi/9)$, $\cos(5\pi/18)$, $1/2$; (III) $1/2$, $\cos(7\pi/18)$, $\cos(4\pi/9)$. (a) HC phase diagram of the three-length-scale model in ϵ - α plane. (b) Stationary patterns of ODQC³ at $\epsilon = -0.01$ and $\alpha = 0.5$. Non-primary RLVs with intensities greater than 10^{-6} are indicated by small dots. (c) Phase diagram of the SC minimal Landau model with three length scales $\cos(\pi/18)$, $\cos(2\pi/9)$, and $1/2$.

ber of three- and four-RLV interactions, resulting in the same HC free energy

$$\begin{aligned}
 \mathcal{F}_{\text{ODQC}^3}(\{\hat{\phi}\}_{j=1}^3, \epsilon^*) &= -9\epsilon^* \sum_{j=1}^3 \hat{\phi}_j^2 - 12 \sum_{j=1}^3 \hat{\phi}_j^3 \\
 &- 36\hat{\phi}_1 \sum_{j=2}^3 \hat{\phi}_j^2 - 36\hat{\phi}_2\hat{\phi}_3(2\hat{\phi}_1 + \hat{\phi}_3) + \frac{459}{2} \sum_{j=1}^3 \hat{\phi}_j^4 \\
 &+ 108\hat{\phi}_2^3(2\hat{\phi}_1 + \hat{\phi}_3) + 216\hat{\phi}_3^3(\hat{\phi}_1 + \hat{\phi}_2) + 702\hat{\phi}_2^2\hat{\phi}_3^2 \\
 &+ 702\hat{\phi}_1^2(\hat{\phi}_2^2 + \hat{\phi}_3^2) + 756\hat{\phi}_1^2\hat{\phi}_2\hat{\phi}_3 + 432\hat{\phi}_1\hat{\phi}_2\hat{\phi}_3(\hat{\phi}_2 + \hat{\phi}_3).
 \end{aligned} \tag{21}$$

Fig. 9(a) plots the HC phase diagram, where ODQC³ is expected to be thermodynamic stable in $-0.0901 \leq \epsilon^* \leq -0.0180$. Moreover, we take the minimal model (I) as an example to examine the thermodynamic stability of ODQCs under SC. By use of the projection method

(see SM Eq. (27) for projection matrix and Fig. 10(f) for high-dimensional coordinates), we obtain the stationary ODQC³ phase. Its diffraction pattern and real-space morphology are shown in Fig. 9(b). Fig. 9(c) presents the SC phase diagram, revealing a stable region for ODQC³. The phase boundaries exhibit a slight shift compared to the HC phase diagram, which may be attributed to the non-negligible influence of non-primary RLVs and the predominant contribution of primary RLVs. Moreover, we find stable ODQC³ in the models (II) and (III) with SC.

IV. Conclusion

In this paper, we propose an efficient method (ISM) to design a minimal Landau theory to stabilize desired QCs. ISM evaluates almost all possible configurations of RLVs for the target QC, allowing us to identify the optimal configuration with the lowest free energy, as the free energy functional can be expressed as a polynomial under HC. With this optimal configuration, ISM then constructs phase diagrams to assess the thermodynamic stability of the target QC. Generally, configurations with more length scales contain more primary RLVs, which can form more three-RLV interactions to lower the free energy. Thus, we can always design a minimal Landau theory to stabilize desired QCs by gradually increasing the number of length scales.

Using ISM, we design minimal Landau theories to stabilize $2n$ -fold QCs ($n = 4, \dots, 9$). Concretely, two-length-scale Landau models can stabilize 10- and 12-fold QCs, which is consistent with previous results. Moreover, we obtain stable 8- and 18-fold QCs in three-length-scale Landau models, reducing the number of length scales compared to earlier studies. Our findings also indicate that three-length-scale models can stabilize 14- and 16-fold QCs. We believe that these minimal models with relatively simple potentials could be helpful to control the synthesis of QCs.

V. Supplementary Material

Table I gives the optimal primary RLVs, the formula of HC free energies, and HC phase diagrams for $2n$ -fold

quasicrystals (QCs) ($n = 4, \dots, 9$). From these HC phase diagrams, one can conclude that the HC minimal models of 10- and 12-fold QCs have two length scales and the HC minimal models of the rest QCs require three length scales.

TABLE I: Optimal primary RLVs, HC free energies, and HC phase diagrams of $2n$ -fold QCs ($n = 4, \dots, 9$). Length scales satisfy $q_j = \cos(w_j\pi/(2n))$, and offset angles are $\theta_j = s_j\pi/(2n)$, where $j = 1, 2, \dots, m$, m is the number of length scales. s_1 defaults to 0. The second to fourth columns correspond to $m = 2, 3, 4$. The parameters of optimal primary RLVs w_j and s_j for different configurations are separated by semicolons. The primary RLVs located on four length scales are marked by magenta \bullet , royal blue \circ , purple \odot , and dark turquoise \otimes , respectively. The specific values of length scales and offset angles are listed at the bottom of the RLV patterns. We also write the HC free energies of desired QCs based on the optimal primary RLVs. In phase diagrams, we use superscripts to denote the number of valid length scales.

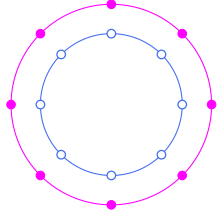
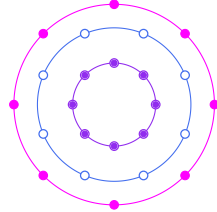
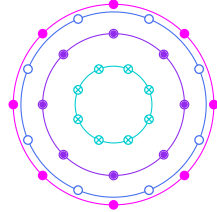
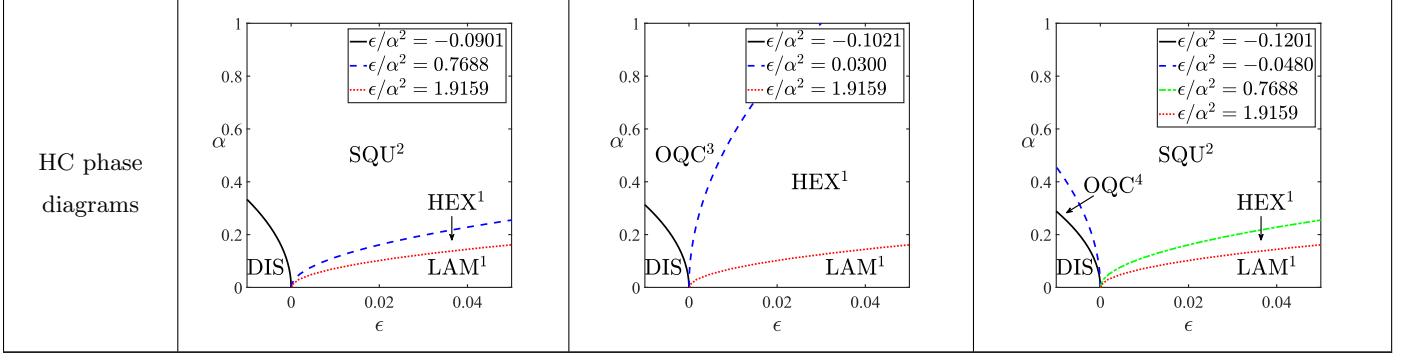
Desired QCs	Octagonal (O) QCs (8-fold)		
$\{w_j\}_{j=1}^m$	0, 2	1, 2, 3	0, 1, 2, 3
$\{s_j\}_{j=1}^m$	0, 0	0, 1, 0	0, 1, 0, 1
Optimal primary RLVs	 <p>$q : 1, \cos \frac{\pi}{4}$ $\theta : 0, 0$</p>	 <p>$q : \cos \frac{\pi}{8}, \cos \frac{\pi}{4}, \cos \frac{3\pi}{8}$ $\theta : 0, \pi/8, 0$</p>	 <p>$q : 1, \cos \frac{\pi}{8}, \cos \frac{\pi}{4}, \cos \frac{3\pi}{8}$ $\theta : 0, \pi/8, 0, \pi/8$</p>
HC free energies	$-4\epsilon^* \sum_{j=1}^2 \hat{\phi}_j^2 - 16\hat{\phi}_1\hat{\phi}_2^2$ $+ 42 \sum_{j=1}^2 \hat{\phi}_j^4 + 120\hat{\phi}_1^2\hat{\phi}_2^2$	$-4\epsilon^* \sum_{j=1}^3 \hat{\phi}_j^2 - 16\hat{\phi}_2(\hat{\phi}_1 + \hat{\phi}_3)^2$ $+ 42 \sum_{j=1}^3 \hat{\phi}_j^4 + 192\hat{\phi}_1\hat{\phi}_2^2\hat{\phi}_3$ $+ 144(\hat{\phi}_1^2\hat{\phi}_2^2 + \hat{\phi}_1^2\hat{\phi}_3^2 + \hat{\phi}_2^2\hat{\phi}_3^2)$ $+ 48\hat{\phi}_1\hat{\phi}_3(\hat{\phi}_1^2 + \hat{\phi}_3^2)$	$-4\epsilon^* \sum_{j=1}^4 \hat{\phi}_j^2 - 16\hat{\phi}_1(\hat{\phi}_3^2 + 2\hat{\phi}_2\hat{\phi}_4)$ $- 16\hat{\phi}_3(\hat{\phi}_2 + \hat{\phi}_4)^2 + 42 \sum_{j=1}^4 \hat{\phi}_j^4$ $+ 48\hat{\phi}_2\hat{\phi}_4(\hat{\phi}_2^2 + \hat{\phi}_4^2) + 120\hat{\phi}_1^2 \sum_{j=2}^4 \hat{\phi}_j^2$ $+ 144(\hat{\phi}_3(\hat{\phi}_1 + \hat{\phi}_3)(\hat{\phi}_2^2 + \hat{\phi}_4^2) + \hat{\phi}_2^2\hat{\phi}_4^2)$ $+ 192\hat{\phi}_2\hat{\phi}_3^2\hat{\phi}_4 + 288\hat{\phi}_1\hat{\phi}_2\hat{\phi}_3\hat{\phi}_4$

Table I (continued): optimal primary RLVs, HC free energies and HC phase diagrams,



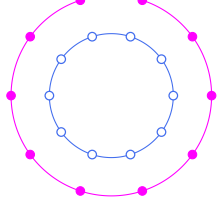
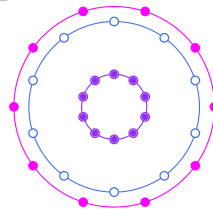
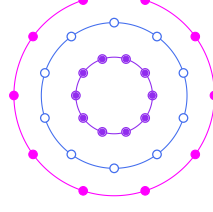
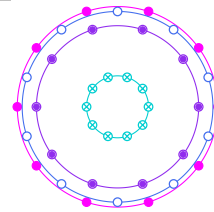
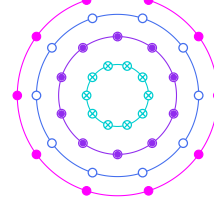
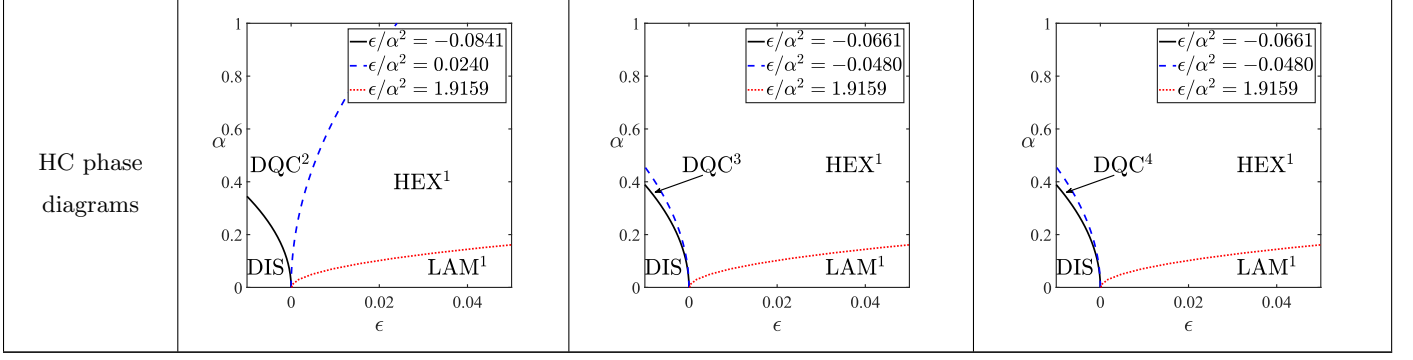
Desired QCs	Decagonal (D) QCs (10-fold)		
$\{w_j\}_{j=1}^m$	1, 3	1, 2, 4; 2, 3, 4	0, 1, 2, 4; 0, 2, 3, 4
$\{s_j\}_{j=1}^m$	0, 0	0, 1, 1; 0, 1, 0	0, 1, 0, 0; 0, 0, 1, 0
Optimal primary RLVs	 <p>$q : \cos \frac{\pi}{10}, \cos \frac{3\pi}{10}$ $\theta : 0, 0$</p>	 <p>$q : \cos \frac{\pi}{10}, \cos \frac{\pi}{5}, \cos \frac{2\pi}{5}$ $\theta : 0, \pi/10, \pi/10$</p>  <p>$q : \cos \frac{\pi}{5}, \cos \frac{3\pi}{10}, \cos \frac{2\pi}{5}$ $\theta : 0, \pi/10, 0$</p>	 <p>$q : 1, \cos \frac{\pi}{10}, \cos \frac{\pi}{5}, \cos \frac{2\pi}{5}$ $\theta : 0, \pi/10, 0, 0$</p>  <p>$q : 1, \cos \frac{\pi}{5}, \cos \frac{3\pi}{10}, \cos \frac{2\pi}{5}$ $\theta : 0, 0, \pi/10, 0$</p>
HC free energies	$-5\epsilon^* \sum_{j=1}^2 \hat{\phi}_j^2 - 20\hat{\phi}_1\hat{\phi}_2(\hat{\phi}_1 + \hat{\phi}_2)$ $+ \frac{135}{2} \sum_{j=1}^2 \hat{\phi}_j^4 + 60\hat{\phi}_1\hat{\phi}_2 \sum_{j=1}^2 \hat{\phi}_j^2$ $+ 210\hat{\phi}_1^2\hat{\phi}_2^2$	$-5\epsilon^* \sum_{j=1}^3 \hat{\phi}_j^2 - 20\hat{\phi}_1\hat{\phi}_2(\hat{\phi}_2 + 2\hat{\phi}_3)$ $+ \frac{135}{2} \sum_{j=1}^3 \hat{\phi}_j^4 + 60\hat{\phi}_2\hat{\phi}_3 \sum_{j=2}^3 \hat{\phi}_j^2$ $+ 210(\hat{\phi}_1^2\hat{\phi}_2^2 + \hat{\phi}_1^2\hat{\phi}_3^2 + \hat{\phi}_2^2\hat{\phi}_3^2)$ $+ 180\hat{\phi}_1^2\hat{\phi}_2\hat{\phi}_3$	$-5\epsilon^* \sum_{j=1}^4 \hat{\phi}_j^2 - 40\hat{\phi}_2\hat{\phi}_4(\hat{\phi}_1 + \hat{\phi}_3)$ $-20\hat{\phi}_2\hat{\phi}_3^2 + \frac{135}{2} \sum_{j=1}^4 \hat{\phi}_j^4$ $+ 60\hat{\phi}_3\hat{\phi}_4 \sum_{j=3}^4 \hat{\phi}_j^2 + 180\hat{\phi}_1^2 \sum_{j=2}^4 \hat{\phi}_j^2$ $+ 180\hat{\phi}_1\hat{\phi}_3(\hat{\phi}_2^2 + \hat{\phi}_4(\hat{\phi}_3 + \hat{\phi}_4))$ $+ 210(\hat{\phi}_2^2\hat{\phi}_3^2 + \hat{\phi}_2^2\hat{\phi}_4^2 + \hat{\phi}_3^2\hat{\phi}_4^2)$ $+ 180\hat{\phi}_2^2\hat{\phi}_3\hat{\phi}_4$

Table I (continued): optimal primary RLVs, HC free energies and HC phase diagrams,



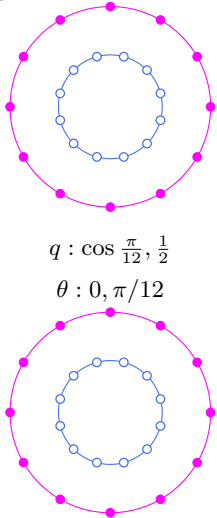
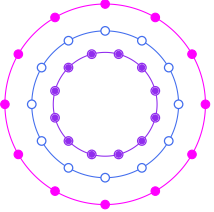
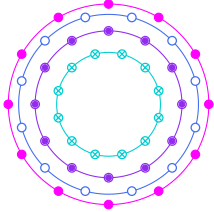
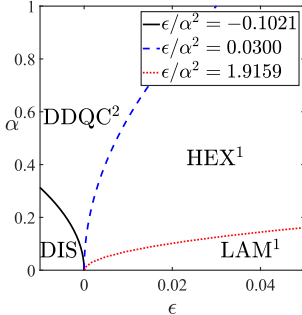
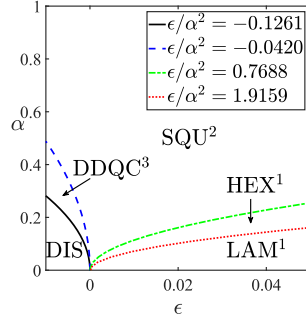
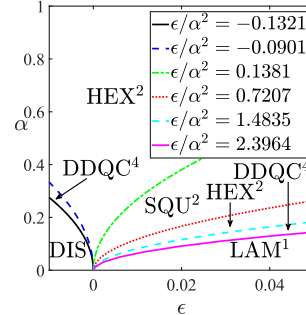
Desired QCs	Dodecagonal (DD) QCs (12-fold)		
$\{w_j\}_{j=1}^m$	1, 4, 4, 5	1, 3, 4	1, 2, 3, 4
$\{s_j\}_{j=1}^m$	0, 1, 0, 1	0, 0, 1	0, 1, 0, 1
Optimal primary RLVs	 <p>$q : \cos \frac{\pi}{12}, \frac{1}{2}$ $\theta : 0, \pi/12$</p> <p>$q : \frac{1}{2}, \cos \frac{5\pi}{12}$ $\theta : 0, \pi/12$</p>	 <p>$q : \cos \frac{\pi}{12}, \cos \frac{\pi}{4}, \frac{1}{2}$ $\theta : 0, 0, \pi/12$</p>	 <p>$q : \cos \frac{\pi}{12}, \cos \frac{\pi}{6}, \cos \frac{\pi}{4}, \frac{1}{2}$ $\theta : 0, \pi/12, 0, \pi/12$</p>

Table I (continued): optimal primary RLVs, HC free energies and HC phase diagrams,

HC free energies	$-6\epsilon^* \sum_{j=1}^2 \hat{\phi}_j^2 - 8(\hat{\phi}_1 + \hat{\phi}_2)^3$ $+ 99 \sum_{j=1}^2 \hat{\phi}_j^4 + 144\hat{\phi}_1\hat{\phi}_2 \sum_{j=1}^2 \hat{\phi}_j^2$ $+ 360\hat{\phi}_1^2\hat{\phi}_2^2$	$-6\epsilon^* \sum_{j=1}^3 \hat{\phi}_j^2 - 8 \sum_{j=1}^3 \hat{\phi}_j^3 - 48\hat{\phi}_1\hat{\phi}_2\hat{\phi}_3$ $- 24\hat{\phi}_3(\hat{\phi}_1^2 + (\hat{\phi}_1 + \hat{\phi}_2)\hat{\phi}_3)$ $+ 99 \sum_{j=1}^3 \hat{\phi}_j^4 + 72\hat{\phi}_1^3(\hat{\phi}_2 + 2\hat{\phi}_3)$ $+ 288\hat{\phi}_1\hat{\phi}_2(\hat{\phi}_1(\hat{\phi}_2 + \hat{\phi}_3) + \hat{\phi}_2\hat{\phi}_3)$ $+ 324\hat{\phi}_2^2\hat{\phi}_3^2 + 360\hat{\phi}_1\hat{\phi}_3^2(\hat{\phi}_1 + \hat{\phi}_2)$ $+ 144\hat{\phi}_3^3(\hat{\phi}_1 + \hat{\phi}_2)$	$-6\epsilon^* \sum_{j=1}^4 \hat{\phi}_j^2 - 8 \sum_{j=1}^4 \hat{\phi}_j^3 - 24\hat{\phi}_1^2\hat{\phi}_4$ $- 24\hat{\phi}_4^2 \sum_{j=1}^3 \hat{\phi}_j - 48\hat{\phi}_1\hat{\phi}_3(\hat{\phi}_2 + \hat{\phi}_4)$ $+ 99 \sum_{j=1}^4 \hat{\phi}_j^4 + 72\hat{\phi}_1^3(\hat{\phi}_3 + 2\hat{\phi}_4)$ $+ 72\hat{\phi}_4^3(2\hat{\phi}_1 + \hat{\phi}_2 + 2\hat{\phi}_3)$ $+ 144\hat{\phi}_1\hat{\phi}_2\hat{\phi}_3(\hat{\phi}_1 + \hat{\phi}_3)$ $+ 216\hat{\phi}_1\hat{\phi}_2(\hat{\phi}_1\hat{\phi}_4 + \hat{\phi}_2\hat{\phi}_3)$ $+ 288\hat{\phi}_1^2(\hat{\phi}_2^2 + \hat{\phi}_3^2) + 288\hat{\phi}_2^2(\hat{\phi}_3^2 + \hat{\phi}_4^2)$ $+ 288\hat{\phi}_1\hat{\phi}_3\hat{\phi}_4(\hat{\phi}_1 + \hat{\phi}_3) + 288\hat{\phi}_1\hat{\phi}_2\hat{\phi}_4^2$ $+ 288\hat{\phi}_2\hat{\phi}_3\hat{\phi}_4(\hat{\phi}_3 + \hat{\phi}_4) + 324\hat{\phi}_3^2\hat{\phi}_4^2$ $+ 360\hat{\phi}_1\hat{\phi}_4^2(\hat{\phi}_1 + \hat{\phi}_3) + 432\hat{\phi}_1\hat{\phi}_2\hat{\phi}_3\hat{\phi}_4$
HC phase diagrams			

Desired QCs	Tetradecagonal (TD) QCs (14-fold)		
$\{w_j\}_{j=1}^m$	1, 3; 1, 5; 3, 5	1, 3, 5	1, 2, 3, 6; 1, 2, 4, 5; 3, 4, 5, 6
$\{s_j\}_{j=1}^m$	0, 0; 0, 0; 0, 0	0, 0, 0	0, 1, 0, 1; 0, 1, 1, 0; 0, 1, 0, 1

Table I (continued): optimal primary RLVs, HC free energies and HC phase diagrams,

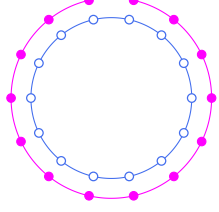
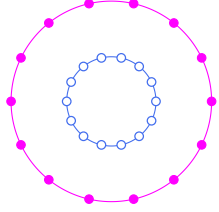
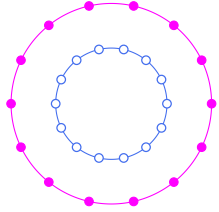
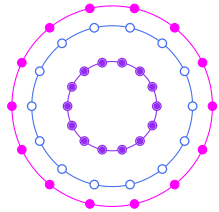
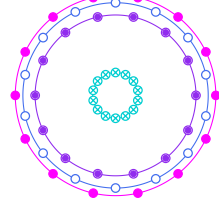
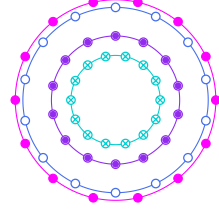
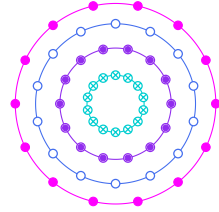
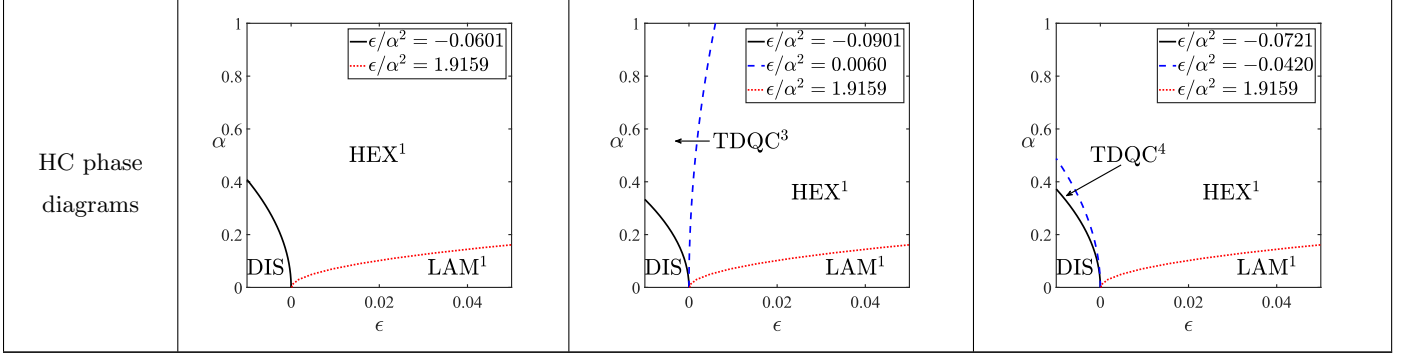
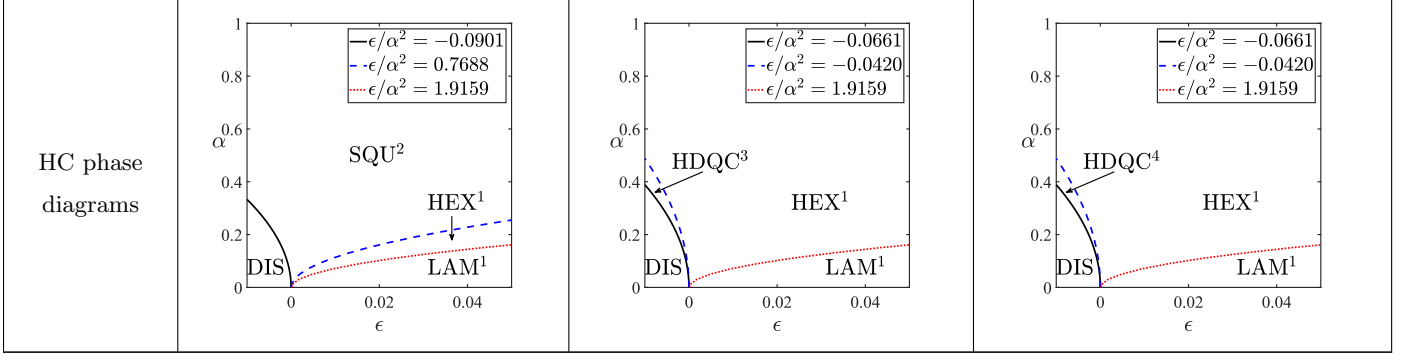
Optimal primary RLVs	 $q : \cos \frac{\pi}{14}, \cos \frac{3\pi}{14}$ $\theta : 0, 0$  $q : \cos \frac{\pi}{14}, \cos \frac{5\pi}{14}$ $\theta : 0, 0$  $q : \cos \frac{3\pi}{14}, \cos \frac{5\pi}{14}$ $\theta : 0, 0$	 $q : \cos \frac{\pi}{14}, \cos \frac{3\pi}{14}, \cos \frac{5\pi}{14}$ $\theta : 0, 0, 0$	 $q : \cos \frac{\pi}{14}, \cos \frac{\pi}{7}, \cos \frac{3\pi}{14}, \cos \frac{3\pi}{7}$ $\theta : 0, \pi/14, 0, \pi/14$  $q : \cos \frac{\pi}{14}, \cos \frac{\pi}{7}, \cos \frac{2\pi}{7}, \cos \frac{5\pi}{14}$ $\theta : 0, \pi/14, \pi/14, 0$  $q : \cos \frac{3\pi}{14}, \cos \frac{2\pi}{7}, \cos \frac{5\pi}{14}, \cos \frac{3\pi}{7}$ $\theta : 0, \pi/14, 0, \pi/14$
HC free energies	$-7\epsilon^* \sum_{j=1}^2 \hat{\phi}_j^2 - 28\hat{\phi}_1\hat{\phi}_2^2 + 84\hat{\phi}_1^3\hat{\phi}_2$ $+ \frac{273}{2} \sum_{j=1}^2 \hat{\phi}_j^4 + 378\hat{\phi}_1^2\hat{\phi}_2^2$	$-7\epsilon^* \sum_{j=1}^3 \hat{\phi}_j^2 - 56\hat{\phi}_1\hat{\phi}_2\hat{\phi}_3$ $- 28(\hat{\phi}_1^2\hat{\phi}_3 + \hat{\phi}_1\hat{\phi}_2^2 + \hat{\phi}_2\hat{\phi}_3^2)$ $+ \frac{273}{2} \sum_{j=1}^3 \hat{\phi}_j^4 + 252\hat{\phi}_1\hat{\phi}_2\hat{\phi}_3 \sum_{j=1}^3 \hat{\phi}_j$ $+ 84(\hat{\phi}_1^3\hat{\phi}_2 + \hat{\phi}_1\hat{\phi}_3^3 + \hat{\phi}_2^3\hat{\phi}_3)$ $+ 378(\hat{\phi}_1^2\hat{\phi}_2^2 + \hat{\phi}_1^2\hat{\phi}_3^2 + \hat{\phi}_2^2\hat{\phi}_3^2)$	$-7\epsilon^* \sum_{j=1}^4 \hat{\phi}_j^2 - 28\hat{\phi}_3(\hat{\phi}_1\hat{\phi}_3 + \hat{\phi}_2^2)$ $- 56\hat{\phi}_2\hat{\phi}_4(\hat{\phi}_1 + \hat{\phi}_3)$ $+ \frac{273}{2} \sum_{j=1}^4 \hat{\phi}_j^4 + 84(\hat{\phi}_1^3\hat{\phi}_3 + \hat{\phi}_2^3\hat{\phi}_4)$ $+ 252\hat{\phi}_3(\hat{\phi}_1\hat{\phi}_2^2 + \hat{\phi}_1\hat{\phi}_4^2 + \hat{\phi}_2\hat{\phi}_3\hat{\phi}_4)$ $+ 378\hat{\phi}_1^2 \sum_{j=2}^4 \hat{\phi}_j^2 + 378\hat{\phi}_2^2 \sum_{j=3}^4 \hat{\phi}_j^2$ $+ 378\hat{\phi}_3^2\hat{\phi}_4^2 + 504\hat{\phi}_1\hat{\phi}_2\hat{\phi}_3\hat{\phi}_4$

Table I (continued): optimal primary RLVs, HC free energies and HC phase diagrams,



Desired QCs	Hexadecagonal (HD) QCs (16-fold)		
$\{w_j\}_{j=1}^m$	0, 4	2, 4, 6	1, 2, 4, 5; 1, 3, 4, 6
$\{s_j\}_{j=1}^m$	0, 0	0, 0, 0	0, 1, 1, 0; 0, 0, 1, 1
Optimal primary RLVs	<p>$q : 1, \cos \frac{\pi}{4}$ $\theta : 0, 0$</p>	<p>$q : \cos \frac{\pi}{8}, \cos \frac{\pi}{4}, \cos \frac{3\pi}{8}$ $\theta : 0, 0, 0$</p>	<p>$q : \cos \frac{\pi}{16}, \cos \frac{\pi}{8}, \cos \frac{\pi}{4}, \cos \frac{5\pi}{16}$ $\theta : 0, \pi/16, \pi/16, 0$</p> <p>$q : \cos \frac{\pi}{16}, \cos \frac{3\pi}{16}, \cos \frac{\pi}{4}, \cos \frac{3\pi}{8}$ $\theta : 0, 0, \pi/16, \pi/16$</p>
HC free energies	$-8\epsilon^* \sum_{j=1}^2 \hat{\phi}_j^2 - 32\hat{\phi}_1\hat{\phi}_2^2$ $+ 180 \sum_{j=1}^2 \hat{\phi}_j^4 + 432\hat{\phi}_1^2\hat{\phi}_2^2$	$-8\epsilon^* \sum_{j=1}^3 \hat{\phi}_j^2 - 32\hat{\phi}_2(\hat{\phi}_1 + \hat{\phi}_3)^2$ $+ 180 \sum_{j=1}^3 \hat{\phi}_j^4 + 96\hat{\phi}_1\hat{\phi}_3(\hat{\phi}_1^2 + \hat{\phi}_3^2)$ $+ 480(\hat{\phi}_1^2\hat{\phi}_2^2 + \hat{\phi}_1^2\hat{\phi}_3^2 + \hat{\phi}_2^2\hat{\phi}_3^2)$ $+ 384\hat{\phi}_1\hat{\phi}_2^2\hat{\phi}_3$	$-8\epsilon^* \sum_{j=1}^4 \hat{\phi}_j^2 - 32\hat{\phi}_2(\hat{\phi}_2\hat{\phi}_3 + \hat{\phi}_4^2)$ $- 64\hat{\phi}_1\hat{\phi}_4(\hat{\phi}_2 + \hat{\phi}_3)$ $+ 180 \sum_{j=1}^4 \hat{\phi}_j^4 + 96\hat{\phi}_1\hat{\phi}_4^3$ $+ 288\hat{\phi}_2(\hat{\phi}_1^2\hat{\phi}_3 + \hat{\phi}_1\hat{\phi}_2\hat{\phi}_4 + \hat{\phi}_3\hat{\phi}_4^2)$ $+ 480\hat{\phi}_1^2 \sum_{j=2}^4 \hat{\phi}_j^2 + 480\hat{\phi}_2^2(\hat{\phi}_3^2 + \hat{\phi}_4^2)$ $+ 480\hat{\phi}_3^2\hat{\phi}_4^2 + 576\hat{\phi}_1\hat{\phi}_2\hat{\phi}_3\hat{\phi}_4$

Table I (continued): optimal primary RLVs, HC free energies and HC phase diagrams,



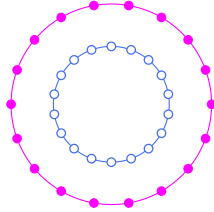
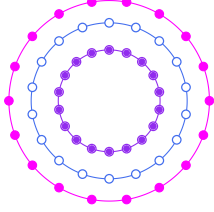
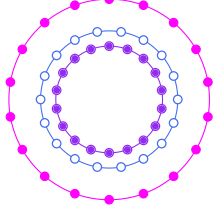
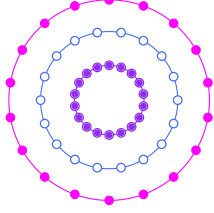
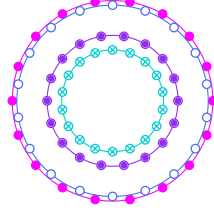
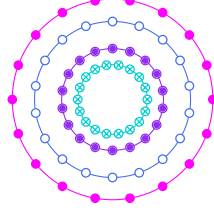
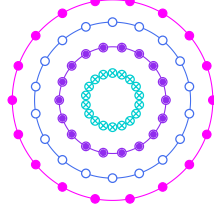
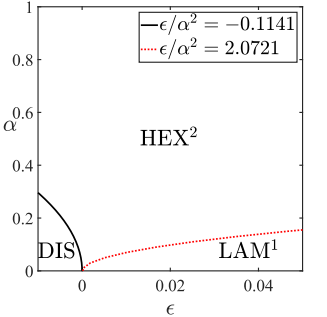
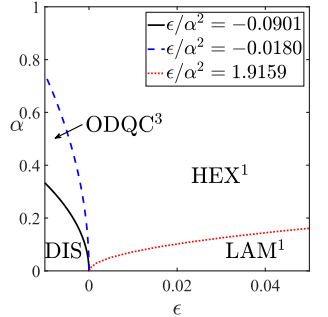
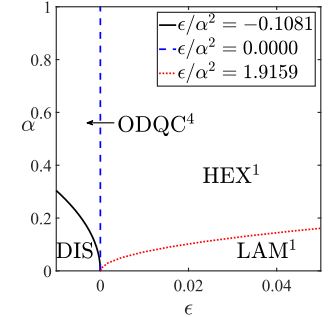
Desired QCs	Octadecagonal (OD) QCs (18-fold)		
$\{w_j\}_{j=1}^m$	3, 6	1, 4, 6; 2, 5, 6; 6, 7, 8	1, 2, 5, 6; 1, 4, 6, 7; 5, 6, 7, 8
$\{s_j\}_{j=1}^m$	0, 1	0, 1, 1; 1, 0, 1; 1, 0, 1	0, 1, 0, 1; 0, 1, 1, 0; 0, 1, 0, 1
Optimal primary RLVs	 <p>$q : \cos \frac{\pi}{6}, \frac{1}{2}$ $\theta : 0, \pi/18$</p>	 <p>$q : \cos \frac{\pi}{18}, \cos \frac{2\pi}{9}, \frac{1}{2}$ $\theta : 0, \pi/18, \pi/18$</p>  <p>$q : \cos \frac{\pi}{9}, \cos \frac{5\pi}{18}, \frac{1}{2}$ $\theta : \pi/18, 0, \pi/18$</p>  <p>$q : \frac{1}{2}, \cos \frac{7\pi}{18}, \cos \frac{4\pi}{9}$ $\theta : \pi/18, 0, \pi/18$</p>	 <p>$q : \cos \frac{\pi}{18}, \cos \frac{\pi}{9}, \cos \frac{5\pi}{18}, \frac{1}{2}$ $\theta : 0, \pi/18, 0, \pi/18$</p>  <p>$q : \cos \frac{\pi}{18}, \cos \frac{2\pi}{9}, \frac{1}{2}, \cos \frac{7\pi}{18}$ $\theta : 0, \pi/18, \pi/18, 0$</p>  <p>$q : \cos \frac{5\pi}{18}, \frac{1}{2}, \cos \frac{7\pi}{18}, \cos \frac{4\pi}{9}$ $\theta : 0, \pi/18, 0, \pi/18$</p>

Table I (continued): optimal primary RLVs, HC free energies and HC phase diagrams,

HC free energies	$ \begin{aligned} & -9\epsilon^* \sum_{j=1}^2 \hat{\phi}_j^2 - 12 \sum_{j=1}^2 \hat{\phi}_j^3 \\ & - 36\hat{\phi}_1 \hat{\phi}_2^2 + \frac{459}{2} \sum_{j=1}^2 \hat{\phi}_j^4 \\ & + 108\hat{\phi}_1 \hat{\phi}_2^3 + 594\hat{\phi}_1^2 \hat{\phi}_2^2 \end{aligned} $	$ \begin{aligned} & -9\epsilon^* \sum_{j=1}^3 \hat{\phi}_j^2 - 12 \sum_{j=1}^3 \hat{\phi}_j^3 \\ & - 36\hat{\phi}_1 \sum_{j=2}^3 \hat{\phi}_j^2 - 36\hat{\phi}_2 \hat{\phi}_3 (2\hat{\phi}_1 + \hat{\phi}_3) \\ & + \frac{459}{2} \sum_{j=1}^3 \hat{\phi}_j^4 + 108\hat{\phi}_2^3 (2\hat{\phi}_1 + \hat{\phi}_3) \\ & + 216\hat{\phi}_3^3 (\hat{\phi}_1 + \hat{\phi}_2) + 702\hat{\phi}_2^2 \hat{\phi}_3^2 \\ & + 702\hat{\phi}_1^2 (\hat{\phi}_2^2 + \hat{\phi}_3^2) + 756\hat{\phi}_1^2 \hat{\phi}_2 \hat{\phi}_3 \\ & + 432\hat{\phi}_1 \hat{\phi}_2 \hat{\phi}_3 (\hat{\phi}_2 + \hat{\phi}_3) \end{aligned} $	$ \begin{aligned} & -9\epsilon^* \sum_{j=1}^4 \hat{\phi}_j^2 - 12 \sum_{j=1}^4 \hat{\phi}_j^3 - 36\hat{\phi}_1 \sum_{j=3}^4 \hat{\phi}_j^2 \\ & - 36\hat{\phi}_2^2 \hat{\phi}_3 - 36\hat{\phi}_4^2 (\hat{\phi}_2 + \hat{\phi}_3) \\ & - 72\hat{\phi}_2 \hat{\phi}_4 (\hat{\phi}_1 + \hat{\phi}_3) + \frac{459}{2} \sum_{j=1}^4 \hat{\phi}_j^4 \\ & + 108\hat{\phi}_1 \hat{\phi}_3 (\hat{\phi}_1^2 + 2\hat{\phi}_3^2) + 216\hat{\phi}_4^3 \sum_{j=1}^3 \hat{\phi}_j \\ & + 108\hat{\phi}_2^3 (2\hat{\phi}_3 + \hat{\phi}_4) + 324\hat{\phi}_1 \hat{\phi}_2^2 \hat{\phi}_3 \\ & + 432\hat{\phi}_1 \hat{\phi}_2 \hat{\phi}_4 (\hat{\phi}_1 + \hat{\phi}_2 + \hat{\phi}_4) \\ & + 432\hat{\phi}_2 \hat{\phi}_3 \hat{\phi}_4 (\hat{\phi}_2 + \hat{\phi}_4) + 594\hat{\phi}_1^2 \hat{\phi}_2^2 \\ & + 702(\hat{\phi}_1^2 + \hat{\phi}_2^2)(\hat{\phi}_3^2 + \hat{\phi}_4^2) \\ & + 702\hat{\phi}_3^2 \hat{\phi}_4^2 + 756\hat{\phi}_2^2 \hat{\phi}_3 \hat{\phi}_4 \\ & + 540\hat{\phi}_1 \hat{\phi}_3 \hat{\phi}_4^2 + 1296\hat{\phi}_1 \hat{\phi}_2 \hat{\phi}_3 \hat{\phi}_4 \end{aligned} $
HC phase diagrams			

Under SC, we further evaluate $2n$ -fold QCs and free energies accurately by the projection method [47]. To be consistent with the rescaling model

$$\begin{aligned}
\mathcal{F}_m[\phi(\mathbf{r})] &= \int \left(-\frac{\epsilon}{2} \phi^2 - \frac{\alpha}{3} \phi^3 + \frac{1}{4} \phi^4 \right) d\mathbf{r} \\
&+ \frac{1}{2} \int \left[\prod_{j=1}^m (\nabla^2 + q_j^2/q_*^2) \phi(\mathbf{r}) \right]^2 d\mathbf{r},
\end{aligned}$$

we measure the length scales of $2n$ -fold QCs in units of q_* . q_* takes the minimal value of $\{q_j\}_{j=1}^m$. Concretely, q_* equals to $\cos(3\pi/8)$ for OQC and HDQC, $\cos(3\pi/10)$ for DQC, $1/2$ for DDQC and ODQC, $\cos(5\pi/14)$ for TDQC.

These projection matrices are

$$\mathcal{P}_{OQC} = \begin{pmatrix} 1 & \cos \frac{\pi}{4} & 0 & \cos \frac{3\pi}{4} \\ 0 & \sin \frac{\pi}{4} & 1 & \sin \frac{3\pi}{4} \end{pmatrix}, \quad (22)$$

$$\mathcal{P}_{DQC} = \begin{pmatrix} 1 & \cos \frac{\pi}{5} & \cos \frac{2\pi}{5} & \cos \frac{3\pi}{5} \\ 0 & \sin \frac{\pi}{5} & \sin \frac{2\pi}{5} & \sin \frac{3\pi}{5} \end{pmatrix}, \quad (23)$$

$$\mathcal{P}_{DDQC} = \begin{pmatrix} 1 & \cos \frac{\pi}{6} & \cos \frac{\pi}{3} & 0 \\ 0 & \sin \frac{\pi}{6} & \sin \frac{\pi}{3} & 1 \end{pmatrix}, \quad (24)$$

$$\mathcal{P}_{TDQC} = \begin{pmatrix} 1 & \cos \frac{\pi}{7} & \cos \frac{2\pi}{7} & \cos \frac{3\pi}{7} & \cos \frac{4\pi}{7} & \cos \frac{5\pi}{7} \\ 0 & \sin \frac{\pi}{7} & \sin \frac{2\pi}{7} & \sin \frac{3\pi}{7} & \sin \frac{4\pi}{7} & \sin \frac{5\pi}{7} \end{pmatrix}, \quad (25)$$

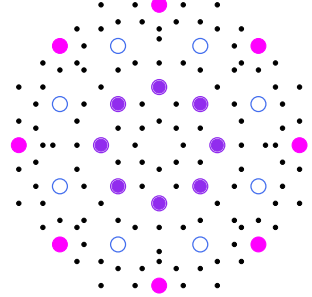
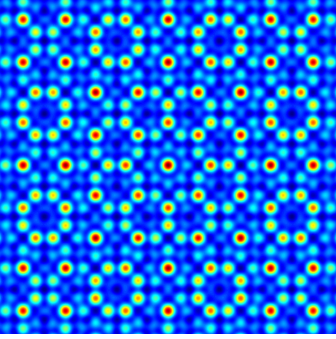
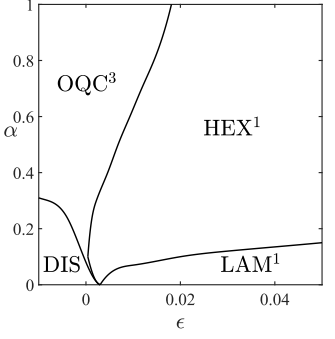
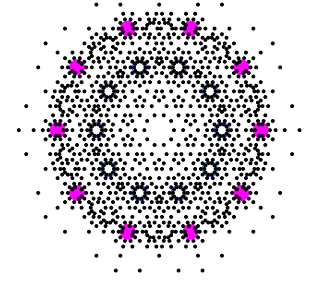
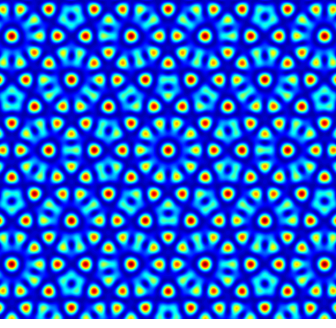
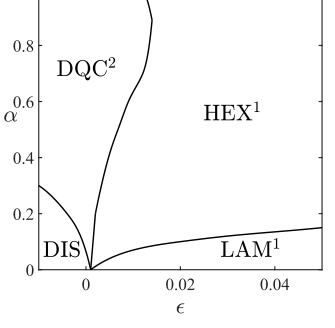
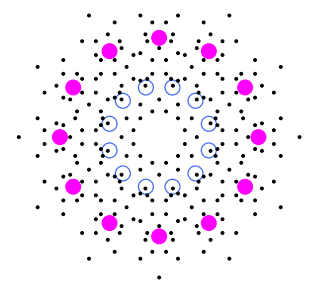
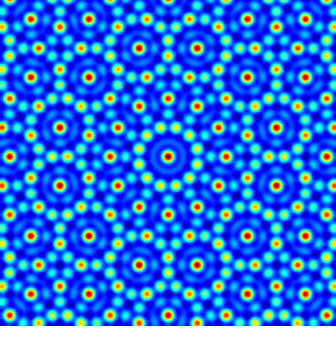
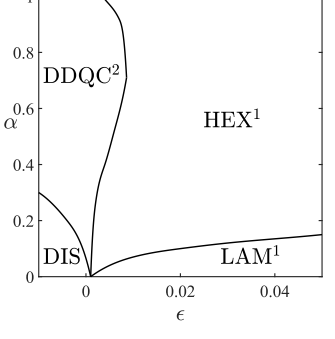
$$\mathcal{P}_{HDQC} = \begin{pmatrix} 1 & \cos \frac{\pi}{8} & \cos \frac{\pi}{4} & \cos \frac{3\pi}{8} & 0 & \cos \frac{5\pi}{8} & \cos \frac{3\pi}{4} & \cos \frac{7\pi}{8} \\ 0 & \sin \frac{\pi}{8} & \sin \frac{\pi}{4} & \sin \frac{3\pi}{8} & 1 & \sin \frac{5\pi}{8} & \sin \frac{3\pi}{4} & \sin \frac{7\pi}{8} \end{pmatrix}, \quad (26)$$

$$\mathcal{P}_{ODQC} = \begin{pmatrix} 1 & \cos \frac{\pi}{9} & \cos \frac{2\pi}{9} & \cos \frac{\pi}{3} & \cos \frac{4\pi}{9} & \cos \frac{5\pi}{9} \\ 0 & \sin \frac{\pi}{9} & \sin \frac{2\pi}{9} & \sin \frac{\pi}{3} & \sin \frac{4\pi}{9} & \sin \frac{5\pi}{9} \end{pmatrix}. \quad (27)$$

In these projection matrices, the number of columns corresponds to the dimensionality of the high-dimensional space. Fig. 10 presents the corresponding high-dimensional coordinates of optimal primary RLVs. In

Table II, we show the stationary patterns and SC phase diagrams of $2n$ -fold QCs. The SC phase diagrams show that the HC minimal models can stabilize desired QCs under SC.

TABLE II: The stationary patterns and SC phase diagrams of $2n$ -fold QCs in the minimal Landau models designed by ISM ($n = 4, \dots, 9$). We apply the projection method to compute these results. Set $\epsilon = -0.01$, $\alpha = 0.4$ for 16-fold QC and $\alpha = 0.5$ for others. We show the diffraction patterns and morphologies of the stationary QCs. Diffraction patterns only plot the RLVs with intensities greater than 10^{-6} . In phase diagrams, we use superscripts to denote the number of valid length scales.

Desired QCs	SC diffraction patterns	SC morphologies	SC phase diagrams
OQCs (8-fold)	 $q : \cos \frac{\pi}{8}, \cos \frac{\pi}{4}, \cos \frac{3\pi}{8}$		
DQCs (10-fold)	 $q : \cos \frac{\pi}{10}, \cos \frac{3\pi}{10}$		
DDQCs (12-fold)	 $q : \cos \frac{\pi}{12}, \frac{1}{2}$		

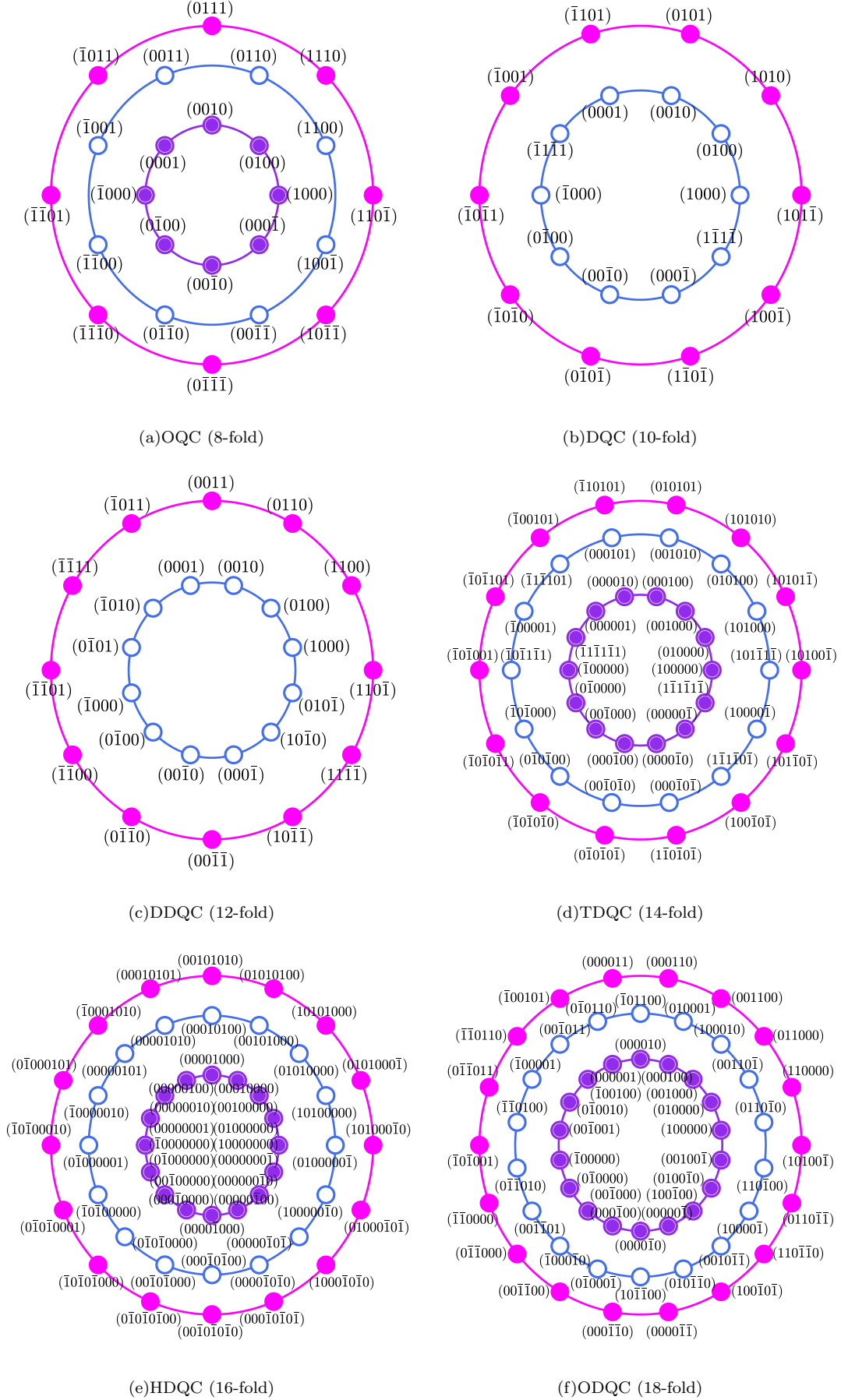
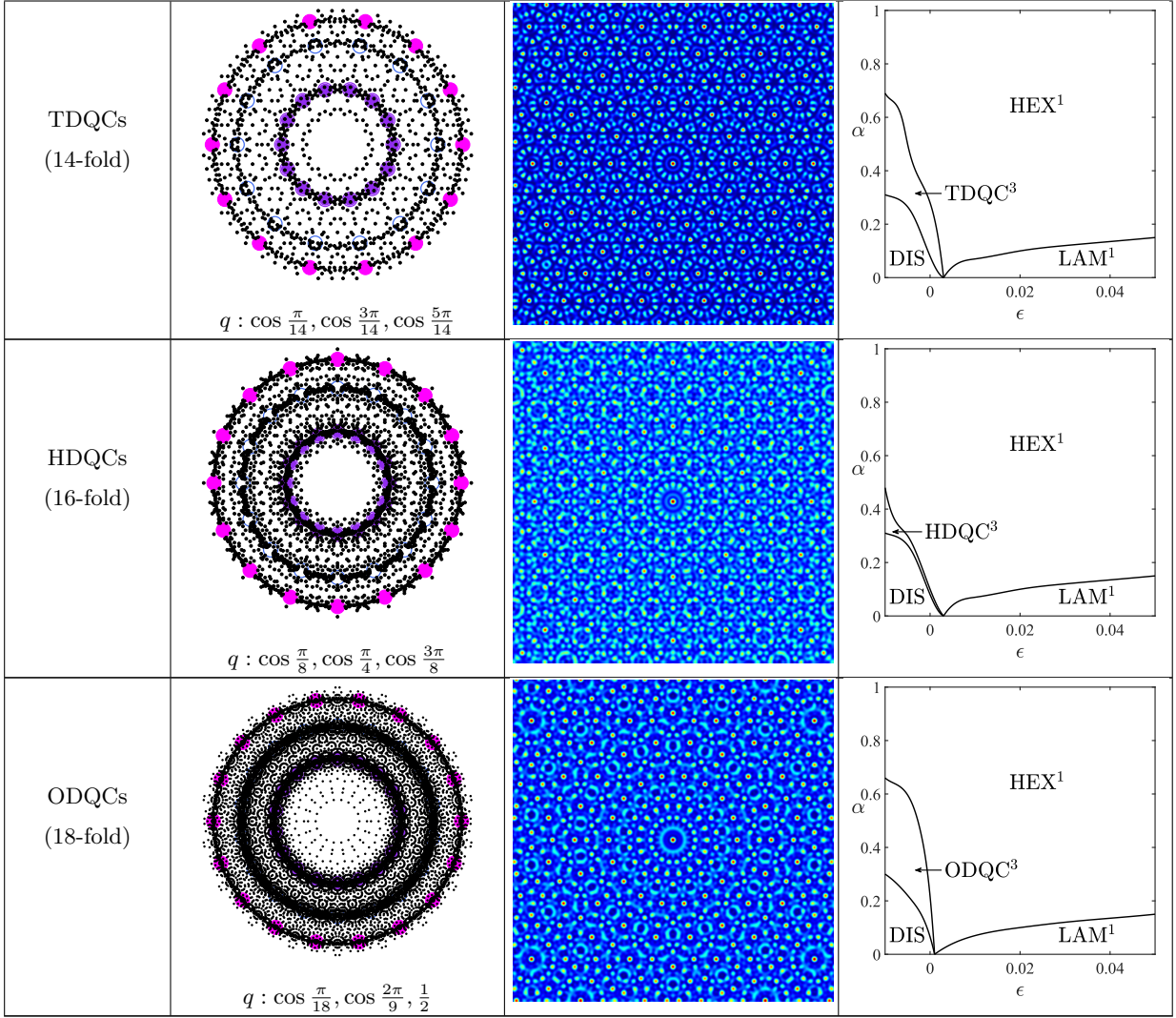


FIG. 10. The high-dimensional coordinates of optimal primary RLVs of $2n$ -fold QCs ($n = 4, \dots, 9$).

Table II (continued): diffraction patterns and morphologies, SC phase diagrams

Table II (continued): diffraction patterns and morphologies, SC phase diagrams



- [1] D. Shechtman, I. Blech, D. Gratias, and J. W. Cahn, *Phys. Rev. Lett.* **53**, 1951 (1984).
- [2] W. Steurer, *Z. Kristallogr.* **219**, 391 (2004).
- [3] X. Zeng, G. Ungar, Y. liu, V. Percec, A. E. Dulcey, and J. K. Hobbs, *Nature* **428**, 157 (2004).
- [4] C. Duan, M. Zhao, Y. Qiang, L. Chen, W. Li, F. Qiu, and A.-C. Shi, *Macromolecules* **51**, 7713 (2018).
- [5] A. J. Archer, T. Dotera, and A. M. Rucklidge, *Phys. Rev. E* **106**, 044602 (2022).
- [6] Y. Liu, T. Liu, X.-Y. Yan, Q.-Y. Guo, H. Lei, Z. Huang, R. Zhang, Y. Wang, J. Wang, F. Liu, F.-G. Bian, E. W. Meijer, T. Aida, M. Huang, and S. Z. D. Cheng, *Proc. Natl. Acad. Sci. USA* **119**, e2115304119 (2022).
- [7] M. Suzuki, T. Orido, A. Takano, and Y. Matsushita, *ACS Nano*. **16**, 6111 (2022).
- [8] X. Zeng, B. Glettner, U. Baumeister, B. Chen, G. Ungar, F. Liu, and C. Tschierske, *Nat. Chem.* **15**, 625 (2023).
- [9] E. Fayen, M. Imp rator-Clerc, L. Filion, G. Foffi, and F. Smallenburg, *Soft Matter* **19**, 2654 (2023).
- [10] H. L wen, *Phys. Rep.* **237**, 249 (1994).
- [11] V. Percec, M. R. Imam, M. Peterca, D. A. Wilson, R. Graf, H. W. Spiess, V. S. Balagurusamy, and P. A.

- Heiney, J. Am. Chem. Soc. **131**, 7662 (2009).
- [12] Y. Cao, A. Scholte, M. Prehm, C. Anders, C. Chen, J. Song, L. Zhang, G. He, C. Tschierske, and F. Liu, *Angew. Chem. Int. Ed.*, e202314454 (2023).
- [13] K. Hayashida, T. Dotera, A. Takan, and Y. Matsushita, *Phys. Rev. Lett.* **98**, 195502 (2007).
- [14] Y. Mai and A. Eisenberg, *Chem. Soc. Rev.* **41**, 5969 (2012).
- [15] J. Zhang and F. S. Bates, *J. Am. Chem. Soc.* **134**, 7636 (2012).
- [16] Q. Xie, Y. Qiang, and W. Li, *ACS Macro. Lett.* **9**, 278 (2020).
- [17] S. Fischer, A. Exner, K. Zielske, J. Petrich, S. Deloudi, W. Steurer, P. Lindner, and S. Företter, *Proc. Natl. Acad. Sci. USA* **108**, 1810 (2011).
- [18] C. G. Sztrum and E. Rabani, *Adv. Mater.* **18**, 565 (2006).
- [19] D. V. Talapin, E. V. Shevchenko, M. I. Bodnarchuk, X. Ye, J. Chen, and C. B. Murray, *Nature* **461**, 964 (2009).
- [20] T. Dotera and T. Gemma, *Philos. Mag.* **86**, 1085 (2006).
- [21] Y. Miyamori, J. Suzuki, A. Takano, and Y. Matsushita, *ACS Macro. Lett.* **9**, 32 (2020).
- [22] A. P. Lindsay, R. M. 3rd Lewis, B. Lee, A. J. Peterson, T. P. Lodge, and F. S. Bates, *ACS Macro. Lett.* **9**, 197 (2020).
- [23] A. P. Tsai, *Sci. Technol. Adv. Mater.* **9**, 013008 (2008).
- [24] M. N. van der Linden, J. P. K. Doye, and A. A. Louis, *J. Chem. Phys.* **136**, 054904 (2012).
- [25] T. Dotera, *Philos. Mag.* **87**, 3011 (2007).
- [26] R. Lifshitz and H. Diamant, *Philos. Mag.* **87**, 3021 (2007).
- [27] K. Barkan, H. Diamant, and R. Lifshitz, *Phys. Rev. B* **83**, 172201 (2011).
- [28] J. Yin, K. Jiang, A.-C. Shi, P. Zhang, and L. Zhang, *Proc. Natl. Acad. Sci. USA* **118**, e2106230118 (2021).
- [29] G. Cui, K. Jiang, and T. Zhou, *arXiv preprint arXiv:2310.07108* (2023).
- [30] C. N. Likos, *Phys. Rep.* **348**, 267 (2001).
- [31] S. A. Brazovskii, *Sov. Phys.-JETP* **41**, 85 (1975).
- [32] J. Swift and P. C. Hohenberg, *Phys. Rev. A* **15**, 319 (1977).
- [33] R. Lifshitz and D. M. Petrich, *Phys. Rev. Lett.* **79**, 1261 (1997).
- [34] B. Echebarria, R. Folch, A. Karma, and M. Plapp, *Phys. Rev. E* **70**, 06160 (2004).
- [35] K. Jiang, P. Zhang, and A.-C. Shi, *J. Phys.: Condens. Matter* **29**, 124003 (2017).
- [36] S. Savitz, M. Babadi, and R. Lifshitz, *IUCrJ.* **5**, 247 (2018).
- [37] K. Jiang and W. Si, *Philos. Mag.* **100**, 84 (2020).
- [38] A. J. Archer, A. M. Rucklidge, and E. Knobloch, *Phys. Rev. Lett.* **111**, 165501 (2013).
- [39] T. Dotera, T. Oshiro, and P. Zihlerl, *Nature* **506**, 208 (2014).
- [40] K. Barkan, M. Engel, and R. Lifshitz, *Phys. Rev. Lett.* **113**, 098304 (2014).
- [41] K. Jiang, J. Tong, P. Zhang, and A.-C. Shi, *Phys. Rev. E* **92**, 042159 (2015).
- [42] P. Subramanian, A. J. Archer, E. Knobloch, and A. M. Rucklidge, *Phys. Rev. Lett.* **117**, 075501 (2016).
- [43] C. Liang, K. Jiang, S. Tang, J. Wang, Y. Ma, W. Liu, and Y. Du, *Cryst. Growth Des.* **22**, 2637 (2022).
- [44] C. Reich, M. Conrad, F. Krumeich, and B. Harbrecht, *MRS Online Proc. Libr.* **553**, 83 (1998).
- [45] S. K. Mkhonta, K. R. Elder, and Z.-F. Huang, *Phys. Rev. Lett.* **111**, 035501 (2013).
- [46] D. J. Ratliff, A. J. Archer, P. Subramanian, and A. M. Rucklidge, *Phys. Rev. Lett.* **123**, 148004 (2019).
- [47] K. Jiang and P. Zhang, *J. Comput. Phys.* **256**, 428 (2014).
- [48] K. Jiang, S. Li, and P. Zhang, *SIAM J. Numer. Anal.* **62**, 353 (2024).
- [49] K. Jiang, W. Si, C. Chen, and C. Bao, *SIAM J. Sci. Comput.* **42**, B1350 (2020).
- [50] C. Bao, C. Chen, and K. Jiang, *CSIAM-AM* **3**, 133 (2022).
- [51] C. Bao, C. Chen, K. Jiang, and L. Qiu, *SIAM J. Numer. Anal.* **62**, 476 (2024).
- [52] K. Jiang and W. Si, *Automatically generating phase diagram (AGPD) 1.0*, Software copyright registration certificate, National Copyright Administration of the People's Republic of China: 2022SR0139033, <https://github.com/KaiJiangMath/AGPD> (2022).
- [53] N. Wang, H. Chen, and K. H. Kuo, *Phys. Rev. Lett.* **59**, 1010 (1987).
- [54] K. Jiang, J. Tong, P. Zhang, and A.-C. Shi, *Phys. Rev.*

E 92, 042159 (2015).